On the Variety of the Spectral and Temporal Behaviors of Long Gamma-Ray Burst Pulses

Felix Ryde[1,2] and Roland Svensson[2]

ABSTRACT

We find and study a variety of the spectral-temporal behavior during the decay phase of the light curve of long and bright pulse structures in gamma-ray bursts (GRBs). Even though only a small fraction of observed bursts exhibit such pulses, these are of interest to study as they reflect individual emission episodes during the burst. We have previously found that for about half of these decays, the instantaneous photon flux is consistent with a power law in time, where the photon flux $\propto$ 1/time. This decay behavior is a consequence of the validity of both a power law correlation between the hardness and the intensity and an exponential correlation between the hardness and the time-integrated intensity, the fluence. Here, we study a complete sample of 25 pulses (having a peak flux in 1 s time resolution of more than 5 photons s^{-1} cm^{-2} and a S/N of 30 in at least 8 time bins) and, specifically, search for other types of decay behaviors. First, we find that a power law gives a better description of the pulse decays than a stretched exponential, the most commonly assumed pulse shape so far. Then we find that about half of the decays behave approximately as 1/time, and the other half approximately as $1/(\text{time})^3$. For a few of the $1/(\text{time})^3$ decays, the two correlations, the hardness-intensity correlation and the hardness-fluence correlation, are constrained and found to be consistent with the light curve decay behavior. For these cases, the hardness-intensity correlation is still a power law while the hardness-fluence correlation is described by a generalized function.

We study and describe these behaviors analytically and examine actual burst data from the complete catalog of the Burst and Transient Source Experiment on the *Compton Gamma Ray Observatory*. Finally, we briefly discuss our results in a physical context.

Subject headings: gamma rays: bursts

[1]Center for Space Science and Astrophysics, Stanford University, Stanford, CA 94305

[2]SCFAB, Stockholm Observatory, SE-106 91 Stockholm, Sweden

1. Introduction

The general idea of the underlying event, the central engine, producing an observed gamma-ray burst (GRB) is the gravitational collapse of a stellar mass object triggering a relativistically expanding fireball and/or a collimated jet. The mechanism of the conversion of the kinetic energy, connected to the outflow, into the observed radiation is not clear. Shocks within the outflow or shocks imposed by the external medium tap the kinetic energy which is transferred to γ-rays through a single or a combination of radiation processes. Signatures of the gamma-ray epoch of the burst are hidden in the time evolution of the intensity (the light curve) and in its spectral behavior. This is especially true for individual emission episodes, pulses, that complex light curves are believed to consist of. Only a small fraction of all bursts exhibit long and smooth pulses that are useful for such investigations. Nevertheless, these have given a number of relations between different observables, which might lead to a deeper understanding of the creation of the γ-rays, by giving clues to and constraining physical models.

Much effort has been devoted to the study of such relations separately, in their own right, while other works study purely the morphology of the light curve (see, for instance, the review by Ryde 1999). However, the spectral and temporal behaviors are intimately connected and should in a proper treatment be studied together. A first such step was made in Ryde & Svensson (2000; hereafter RS00) who gave a self-consistent description, describing the complete spectral-temporal behavior of the decay phase of a pulse structure in the light curve. RS00 described, in detail, the most common behavior found in $\sim 45\%$ of long bright GRB pulses. It is of specific interest to study the decay phase of a pulse structure, as it most probably describes a certain radiative regime of the emission; for instance, it could contain information on the actual cooling of the emitting region. In the present paper, we explore the approach outlined in RS00 and search for other types of spectral/temporal behaviors, guided by the variety of behaviors of the light curve.

Throughout this paper, we adopt the following notation. $E_{\rm pk}$ is the peak energy of the spectrum, defined as the photon energy where the power output is the largest, i.e., the maximum of the $E^2N_{\rm E}$ spectrum, where E is the photon energy in keV and $N_{\rm E}$ is the specific photon flux (photons cm^{-2} s^{-1} keV^{-1}). $N(t)$ is the photon flux at time t (photons cm^{-2} s^{-1}), and finally, $\Phi(t)$ is the photon fluence in cm^{-2}, defined by $\Phi(t) = \int^t N(t')\,dt'$.

For the spectral and temporal evolution there are the following three main observables to study, $E_{\rm pk}(t)$, $N(t)$, and the derived quantity, $\Phi(t)$, neglecting a possible evolution of the instantaneous *shape* of the spectrum. The relations between these three observables are given by two correlations, chosen here as $E_{\rm pk}(N)$ and $E_{\rm pk}(\Phi)$. The most common types of these two correlations are $E_{\rm pk}(N)$ being a power law function of N, and $E_{\rm pk}(\Phi)$ being

an exponential function of Φ. One of the most important issues emphasized in RS00 is that there is an inevitable spectral/temporal connection, something that is not usually considered. For instance, RS00 showed that by combining these two empirical correlations, $E_{\rm pk}(N)$ and $E_{\rm pk}(\Phi)$, one obtains a specific power law decay behavior of $N(t)$ and $E_{\rm pk}(t)$, where the $N(t)$-decay $\propto t^{-n}$ has a power law index $n = 1$.

Knowing two of the four behaviors, $N(t)$, $E_{\rm pk}(t)$, $E_{\rm pk}(N)$, $E_{\rm pk}(\Phi)$, gives the other two. The question is which two of the four are the most fundamental ones. The way the research field has developed is that the two empirical correlations were established first. It has, on the other hand, not been obvious with which functional shape to fit the pulse light curve, $N(t)$. The most commonly assumed pulse shape is that of a stretched exponential, but there has been no motivation for this other than that it is a flexible pulse shape when making fits over the entire pulse. Essentially no work has been done on fitting $E_{\rm pk}(t)$. With this history, we focus on the three previously studied behaviors, $N(t)$, $E_{\rm pk}(N)$, $E_{\rm pk}(\Phi)$.

Since the light curve is much better suited for statistical analysis, since the noise (Poisson statistics) is relatively small (as compared to the two correlations), we study what different shapes, $N(t)$, of the light curve lead to, assuming that one of the two empirical relations, $E_{\rm pk}(N)$ or $E_{\rm pk}(\Phi)$, is valid. The search is rigidly guided by the actual GRB observations, which is complemented by an analytical treatment. Some of the results have been presented in a preliminary form in Ryde & Svensson (2001).

In § 2, we discuss the shape of individual pulses in the GRB light curve, comment on the two common correlations, a power law $E_{\rm pk}(N)$ and an exponential $E_{\rm pk}(\Phi)$, describing the spectral evolution over time of such pulses, and, finally, what results for $N(t)$ and $E_{\rm pk}(t)$ the combination of these two correlations give rise to. The observations, made with the Burst And Transient Source Experiment (BATSE) on the *Compton Gamma-Ray Observatory (CGRO)*, and how the complete pulse sample was selected from the 9 years of operation are discussed in § 3. In § 4, we analyze the 25 light curve decays, and conclude that they are better described by a power law decay rather than by a stretched exponential. The decay index, n, turns out to have a bimodal distribution, with approximately half the pulses having $n \sim 1$ and the other half having $n \sim 3$ but with a wide spread. This leads us in § 5 to generalize the analytical treatment in RS00, to cases with $n \neq 1$. These results are then used in § 6, to fit the data for three different cases. These are:

i) the two correlations are given by a power law $E_{\rm pk}(N)$ and an exponential $E_{\rm pk}(\Phi)$, consequently the power law pulse decay has the index $n = 1$;

ii) the pulse decay, $N(t)$, is fitted as a power law of index n, the exponential $E_{\rm pk}(\Phi)$ is assumed to be valid, and a fit is made to the generalized $E_{\rm pk}(N)$ of § 5; and finally

iii) the pulse decay, $N(t)$, is fitted as a power law of index n, the power law $E_{\rm pk}(N)$ is assumed to be valid, and a fit is made to the generalized $E_{\rm pk}(\Phi)$ of § 5.

We study, in particular, the 11 cases with $n \sim 3$, and find that about half preferably belongs to case ii) and the other half to case iii). Furthermore, we re-analyze these 11 pulse decays by relaxing n to be free in the fitting of the generalized correlations. Only four pulses are then sufficiently constrained and they are all consistent with a power law $E_{\rm pk}(N)$ and that $E_{\rm pk}(\Phi)$ is given by the generalized function of § 5. In § 7, we elude on a few points in our analysis and discuss our results in a physical context. We finish off by summarizing our results in § 8.

2. Temporal and Spectral Behavior of a GRB

2.1. Shape of the Light Curve

A remarkable feature of the observed properties of GRBs is the large diversity of the light curves, both morphologically and in strength and duration. Different approaches to understanding the light curve morphology have been pursued. It is generally believed that the fundamental constituent of a GRB light curve is a time structure, a pulse, having a sharp rise and a slower decay phase, with the decay rate decreasing smoothly (e.g., Fishman et al. 1994; Norris et al. 1996; Stern & Svensson 1996). This shape is denoted by the acronym FRED, fast-rise and exponential-decay, even though the decay is not necessarily exponential. A burst can consist of only a few such pulses, clearly separable, producing a simple and smooth light curve. In the same manner, complex light curves are superpositions of many such fundamental pulses. Mixtures of the two types are also common. Such interpretations have been shown to be able to explain and partly reproduce many observed light curve morphologies. To reveal the underlying process of GRBs, the fundamental pulses are of special interest as they probably show the clearest signature of the underlying physics.

To model the morphological shape of a *whole* pulse, i.e., its location in time, the amplitude, the width, the rise phase, the transition phase, and the decay phase, a "stretched" exponential is often used:

$$N(t) = N_0 e^{-(|t-t_{\rm max}|/\tau_{\rm r,d})^{\nu}}, \tag{1}$$

where $t_{\rm max}$ is the time of the maximum photon number flux, N_0, of the pulse, $\tau_{\rm r,d}$ are the time constants for the rise and the decay phases, respectively, and ν is the peakedness

parameter[3]. Such a function gives a flexibility which makes it possible to describe the whole shape of most pulses, and to quantify the characteristics of the pulses for a statistical analysis. Norris et al. (1996) studied a sample of bursts observed by the BATSE Large Area Detectors (LADs) and stored in four energy channels[4]. They modeled the light curves in detector counts in the four channels separately and found that the decay generally lies between a pure exponential ($\nu = 1$) and a Gaussian ($\nu = 2$). Lee et al. (1998) studied approximately 2500 pulse structures, in individual energy channels, using the high time resolution BATSE TTS data type, modeling them with the stretched exponential function of equation (1). They confirmed the general behavior that pulses tend to have shorter rise times than decay times. Norris et al. (1996) also used equation (1) to create an algorithm to separate overlapping pulses based on χ^2 fitting. Scargle (1998) introduced an algorithm based on Bayesian principles to estimate the characteristics of a pulse (location in time, amplitude, width, and rise and decay times). This method has the advantage that it is independent of any explicit pulse shape model and exploits the full time resolution of the data.

In general, the rise and decay phases of a radiation pulse give us different aspects of the emitting region. In the case of a region becoming active, the rise phase describes the size of the region while the decay phase is determined by the cooling of it. To understand the radiation process involved in the cooling, it is of interest to concentrate the study to the decay phase. Schaefer & Dyson (1996) studied the decay phase of 10 smooth FRED pulses in the four BATSE energy channels separately and found that most of them are not exponentials, although a few cases come close. A power-law fit passes most of their statistical tests. Indeed, in the description of RS00, on which we base the present work, the decay phase of a pulse is described with $N(t) = N_0/(1 + t/\tau)$, where $t = 0$ is the start of the decay phase where $N(t) = N_0$. This will be discussed, in detail, in §2.3. However, for such a behavior the fluence is divergent

$$\Phi(t) = N_0 \tau \ln(1 + t/\tau) \tag{2}$$

and therefore the decay of the intensity must eventually change into a more rapid one, or possibly be turned off completely.

It is thus an important issue to understand the actual duration of individual pulses, for instance, for the interpretation of GRB light curves as being a superposition of individual pulses. Giblin et al. (1999) report on GRB 980923 (BATSE trigger 7113) as having an

[3]For $\nu > 1$, equation (1) is, strictly speaking, a compressed exponential.

[4]See Fishman et al. (1989), for a description of the different data types of the BATSE data.

apparent transition from a prompt, relatively short and variable phase to a longer and smoother decay. They interpret this as the onset of the afterglow emission seen subsequently at other wavelengths. Furthermore, Stern (1999) showed a few examples of GRB pulses with near-exponential tails that are traceable over almost 4 orders of magnitude in intensity. Stern (1999) argues that nonlinear properties of an optically thick pair plasma could produce this. When the emitting system is turned off, the large pair optical depth can disappear quickly as the plasma annihilates on the short time scale of a few light crossing times. There are several examples of light curves which can be interpreted as having a sudden change, going into a more rapid decay (see, e.g., the left-hand panels in Figure 8 below for triggers 829 and 6630).

2.2. Correlations of the Spectral Evolution

The first important relation between the observables, $E_{\rm pk}$, N, and Φ, is the correlation between the instantaneous, integrated intensity, N, and the hardness of the spectrum, $E_{\rm pk}$, the Hardness-Intensity Correlation (HIC). A common behavior is a tracking between the intensity and the hardness, first noted by Golenetskii et al. (1983), who described it quantitatively as a power-law relation between the instantaneous luminosity ($\propto$ the energy flux) and the peak energy

$$L \propto (kT)^{\gamma}, \tag{3}$$

where the peak of the spectrum was quantified as the temperature in the thermal bremsstrahlung model (k is the Boltzmann's constant). The power-law index (the correlation index), γ, was found to have typical values of $1.5 - 1.7$. Kargatis et al. (1994), confirmed the existence of such a HIC. Special interest has been focused on the HIC behavior over the decay phase of individual pulses in the GRB light curve. Kargatis et al. (1995) found a power law HIC in 28 pulse decays in 15 out of 26 GRBs with prominent pulses. Furthermore, in their study of the decay phase of GRB pulses, RS00 gave an alternative description of the HIC:

$$E_{\rm pk}(N) = E_{\rm pk,0}(N/N_0)^{\delta}, \tag{4}$$

where δ is the correlation index. Finally, Borgonovo & Ryde (2001) studied a sample of 82 GRB pulse decays and found them to be consistent with a power law HIC in, at least, 57% of the cases and for these found $\gamma = 1.9 \pm 0.75$. They also found that the power law indices from pulses within a burst are more alike as compared to the distribution of indices from pulses in different bursts.

The second empirical relation, the Hardness-Fluence Correlation (HFC), defines how the instantaneous spectrum evolves as a function of photon fluence. Liang & Kargatis

(1996) found an HFC for individual pulses in which the power peak energy, $E_{\rm pk}$, of the time-resolved spectra decays exponentially as a function of the photon fluence Φ, i.e.,

$$E_{\rm pk}(\Phi) = E_{\rm pk,max} e^{-\Phi/\Phi_0}, \tag{5}$$

where $E_{\rm pk,max}$ is the maximum value of $E_{\rm pk}$ within the pulse, and Φ_0 is the exponential decay constant. The photon fluence is the photon flux integrated from the time of $E_{\rm pk,max}$. The authors found that 35 of the 37 pulses in the study were consistent or marginally consistent with the relation. Furthermore, they concluded that the decay constant is constant from pulse to pulse within a GRB. This view was, however, challenged by Crider et al. (1998) who dismissed the apparent constancy as consistent with drawing values out of a narrow statistical distribution of Φ_0, which they found to be log-normal with a mean of $\log\Phi_0 = 1.75 \pm 0.07$ and a FWHM of $\Delta\log\Phi_0 = 1.0 \pm 0.1$. This result is probably affected by selection effects. They studied a larger sample, including 41 pulses within 26 bursts, by using the algorithm introduced by Norris et al. (1996) to identify pulses. Another approach was also introduced, in which they used the energy fluence instead of the photon fluence. The two approaches are very similar and do not fundamentally change the observed trends of the decay. These results confirm the correlation and extend the number of pulses in which the correlation is found. The exponential HFC $E_{\rm pk}(\Phi)$ was also used by Ryde & Svensson (1999) in their analytical derivation of the shape of the time-integrated spectrum of an entire pulse decay, taking the spectral evolution into account.

2.3. Self-consistent Description of the Evolution

A major step for quantifying the spectral/temporal behavior of GRBs was taken by RS00, where the combination of the two correlations, i.e., the HIC $E_{\rm pk}(N)$ and the HFC $E_{\rm pk}(\Phi)$ as given by equations (4) and (5) was studied. Neither of these correlations includes any explicit time dependence of the spectral evolution. However, combined they do, as the fluence, Φ, is the time integral of the flux, N. This was used in RS00 to synthesize and find a compact and quantitative description of the time evolution of the decay phase of a GRB pulse. They showed that a *power law* HIC $E_{\rm pk}(N)$ and an *exponential* HFC $E_{\rm pk}(\Phi)$ result in the decay phase of the pulse following power-law behaviors:

$$N(t) = \frac{N_0}{(1+t/\tau)}; \tag{6}$$

$$E_{\rm pk}(t) = \frac{E_{\rm pk,0}}{(1+t/\tau)^{\delta}}, \tag{7}$$

where the initial values at the start of the pulse decay are $(N_0, E_{\rm pk,0})$ and the number of additional parameters is limited to two, the time constant τ (where $N[t=\tau] = N_0/2$) and

the HIC index δ. Note that the origin of the time variable, t, is at the start of the decay. The peak energy has a similar dependence as the intensity, differing only in the correlation index δ. Note also that equations (6) and (7) are segments of power law decays with their formal origins of infinite $N(t)$ and $E_{\rm pk}(t)$ at $t = -\tau$. The exponential decay constant of the HFC $E_{\rm pk}(\Phi)$, introduced and defined by Liang & Kargatis (1996), is given by $\Phi_0 \equiv N_0\tau/\delta$, and thus the characteristic time scale of the decay, the time constant, $\tau \equiv \delta\Phi_0/N_0$. Finally, calculating $\Phi(t) = \int N(t')dt'$ gives rise to equation (2). The formulation, given by equations (6) and (7), is equivalent to the two empirical relations, equations (4) and (5), both of which have been proven to be valid in many cases. RS00 studied a complete sample of 83 GRB pulses in this context, fitting both of the original two correlations, as well as the new equivalent formulation and found that this behavior is common (i.e., in 45 % of the pulse decays).

In this work, we will analyze in detail the cases which do not follow the standard description given by equations (6) and (7). According to the results in RS00, a pulse light curve that does not show this time behavior will, by necessity, have a different HIC $E_{\rm pk}(N)$ and/or HFC $E_{\rm pk}(\Phi)$.

3. Data and Methods

3.1. Observations

Our work was conducted on data taken by BATSE on board the *CGRO* (Fishman et al. 1989) during its entire mission from April 1991 until June 2000. BATSE consisted of eight modules placed on each corner of the satellite, which gave full sky coverage. The modules comprised two types of detectors: the Large Area Detector (LAD) and the Spectroscopy Detector (SD). The former had a larger collecting area and was suited for spectral continuum studies, while the latter was designed for studies of spectral features (lines). For our spectral analysis we used the high energy resolution (HER) background and burst data types from the LADs which have 128 energy channels. The burst data have a time resolution in multiples of 64 ms. The *CGRO* Science Support Center (GROSSC) at Goddard Space Flight Center (GSFC) provides these data as processed, high-level products in its public archive. Data are available for all the detectors that triggered on the bursts (often 3 or 4 of the detectors closest to the line-of-sight to the burst location). Models of the relevant Detector Response Matrix (DRM) for each observation are also provided (Pendleton et al. 1995). The eight modules of BATSE made it possible to localize the GRB, which is important since the DRM depends on the source-to-detector axis angle.

We also used the concatenated 64 ms resolution LAD data for visual inspection of the light curve. These data are also provided by GROSSC, and are a concatenation of the three BATSE data types: DISCLA, PREB, and DISCSC.

3.2. Selection of the Sample

To select a complete sample of strong bursts, we started by selecting the bursts in the Current BATSE Catalog[5], up to GRB 000526 (BATSE trigger 8121), for which it is possible to measure peak fluxes. These are approximately 80% of the total 2702 bursts observed. The reason that the peak flux is not measured for the remaining bursts is data gaps and/or missing data types. The Current BATSE Catalog is preliminary, but bursts up to GRB 960825 (trigger 5586) were published in the 4th BATSE Catalogue (Paciesas et al. 1999). The threshold we chose for accepting a burst was that the peak flux (50–300 keV in 1.024 s time resolution) must be more than 5 photons s^{-1} cm^{-2}, which resulted in a set of 190 bursts.

This set was examined visually, burst by burst, using the concatenated 64 ms resolution data. We searched for bursts containing long pulse structures with a general "fast rise-slow decay" shape, often referred to as "fast rise-exponential decays" (FREDs). No analytical function describing the pulse shape was assumed. The reason for using such a loose definition is to have a sample that is independent of any preconceived idea of the pulse shape. The whole selection procedure is similar to the one made in Borgonovo & Ryde (2001).

For the time-resolved spectroscopy, we use a signal-to-noise (S/N) ratio of the observations of ≥ 30, which leads to light curves consisting of only a few broad time bins. To perform detailed time-resolved spectroscopy it has been shown that a $S/N \sim 45$ is needed (Preece et al. 1998). We apply this as much as possible. However, since the aim of our spectral analysis on every time bin is mainly to determine the peak energy as a measure of the hardness and to deconvolve the count spectrum to find the photon flux, we allow ourselves to use a lower S/N, sometimes as low as 30 for weak bursts. In these cases, we check that the results are consistent with higher S/N ratios. This gives us the possibility to study the burst pulses with higher time-resolution, especially for the later time bins.

We need as many time bins as possible to study the spectral evolution. For this purpose, we adopt the criterion that the decay phase of the pulses should have at least 8

[5]http://www.batse.msfc.nasa.gov/batse/

time bins with $S/N = 30$ to be included in the study.

These criteria resulted in a sample of 25 pulses within 23 bursts, i.e., $\approx 1\%$ of the original BATSE catalog. This set is presented in Table 1, where the bursts are denoted by both their BATSE catalog and trigger numbers. In this Table, there is also information on the detector from which the data were taken, the time interval, and the number of time bins ($n_{\rm bins}$) with which each pulse decay was studied (see also the Discussion in § 7). Note that the time variable starts at the trigger time.

3.3. Spectral Modeling

The central part of the analysis was performed with the WINGSPAN package, version 4.4.1 (Preece et al. 1996), provided by the *CGRO* Science Support Center at GSFC. The spectral fitting was done using the MFIT package, version 4.6, running under WINGSPAN. We always chose the data taken with the detector which was closest to the line-of-sight to the GRB, as it has the strongest signal (see Table 1 for the individual cases). The broadest energy band with useful data was selected, often $25 - 1900$ keV. A background estimate was made using the HER data, which consist of low time-resolution measurements ($16 - 500$ s) stored between triggers. The light curve of the background during the outburst was modeled by interpolating these data, approximately 1000 s before and after the trigger, using a polynomial fit, typically of second or third order.

For each time bin to be studied, the photon spectrum with the background subtracted, $N_{\rm E}(E)$, is then determined by using the forward-folding technique. An empirical spectral model is folded through the appropriate DRM and is then fitted by minimizing the χ^2 (using the Levenberg-Marquardt algorithm, see, e.g., Press et al. 1992) between the model count spectrum and the observed count spectrum, giving the best-fit spectral parameters and the normalization. The spectra were modeled with the empirical function (Band et al. 1993):

$$N_{\rm E}(E) = \begin{cases} A\ E^{\alpha} e^{-E/E_0} & \text{if } (\alpha - \beta)E_0 \geq E \\ A' E^{\beta} & \text{if } (\alpha - \beta)E_0 < E\ , \end{cases} \tag{8}$$

where E is the photon energy, E_0 is the $e-$folding energy, α and β are the asymptotic power law indices, A is the amplitude, and A' has been chosen to make the photon spectrum $N_{\rm E}(E)$ a continuous and a continuously differentiable function through the condition

$$A' = A\,[(\alpha - \beta)E_0]^{\alpha-\beta}\, e^{-(\alpha-\beta)}. \tag{9}$$

The power law indices, α and β, were always left free to vary. The photon energy, $E_{\rm pk}$, at which the $E^2 N_{\rm E}$-spectrum peaks, is used as a measure of the spectral hardness instead of

E_0. These are related through $E_{\rm pk} = (2+\alpha)E_0$ and a peak exists only when $\beta < -2$. The photon spectrum arrived at is model-dependent. However, as the Band et al. function (eq. [8]), often gives a good model of the spectra, the photon spectrum found by deconvolving the count spectrum should correspond well with the true photon spectrum. The fitting procedure then has 4 free parameters: A, α and β, and $E_{\rm pk}$. For every time bin, the instantaneous, integrated photon flux, $N(t)$, is found by integrating the modeled photon spectrum ($N_{\rm E}$) over the available energy band of the detector.

We start off by analyzing the light curves in the sample with the non-linear Levenberg-Marquardt method with the statistical weights given by the observed errors.

4. Analysis of the Decays of the Pulse Light Curves

The main target of this study is the early decay phases of long, bright pulses. Apart from the discussion in § 2.1 on possible changes in the decay rate of the light curve, there are additional reasons to be cautious when deciding which time interval should be used in the study. Firstly, we are studying the deconvolved (photon) spectra which often eventually become affected by the limited energy range of the detector. Secondly, to achieve the required S/N ratio, late time bins often become relatively broad. The time assigned to this flux data point is in the middle of the time bin, which, in general, is not exactly correct, and thus can affect details in the analysis. The time interval and the number of time bins used in the statistical analysis for each pulse in the study are shown in Table 1.

As discussed in § 2.1, there is no consensus on what shape the pulse decays of the photon flux have. Both stretched exponentials and power law decays have been used to fit the data. We therefore fit the light curves of our complete sample with the following two general functions; a generalized power law decay:

$$N(t) = \frac{N_0}{(1+t/\tau)^n}, \tag{10}$$

(of which eq. [6] is the special case, $n = 1$), and the stretched exponential decay of equation (1).

The results of the fits of the decay phases in the sample are given in Tables 2, 3, and 7. Table 2 (see also Fig. [8]) gives the results of the fits to equation (10) for every pulse, i.e., the parameters N_0, τ, and n, as well as the reduced χ^2 values of the fits. In Table 3, the parameter values, N_0, $\tau_{\rm d}$, and ν, from the fit to equation (1), are given for all pulses. The χ^2 values in these two Tables should be judged with some caution due to the reasons mentioned above. Furthermore, overlapping and unresolved, minor pulses, which are not

modeled, could also be present. Comparison between fits are still instructive and the overall conclusion is, nevertheless, that the power law function is a better description (having a lower χ^2 value) of the pulse decays than a stretched exponential in all cases but three (triggers 1085, 1625, and 3765). In these three cases, however, the stretched exponential function is only marginally better. In an additional two cases, triggers 973 and 1121, the power law function is not constrained at all. Both of these cases have a large peakedness parameter ($\nu > 1$), i.e., they have an exponential or faster decay, and, in fact, the stretched exponential of equation (1) provides a good fit.

In Figure 8, a continuous histogram of the power law index, n, found for the pulses in the sample is shown. The histogram is constructed by summing Gaussian functions which have the values of the mean and the variance found from the fits. In this Figure, the specific spectral-temporal behavior discussed in RS00 is clearly seen as the peak at $n \sim 1$. The second important result given by this analysis is the apparent bimodal distribution of the index n, in which there is a second maximum close to $n = 3$. The width is larger here, since the larger the n values are, the larger the uncertainties in the measurements are. The number of cases are approximately the same (11 and 12 cases) above and below $n \sim 2$. As the behavior with $n \sim 1$ is apparently not ubiquitous, we will explore analytically other types of analytical spectral/temporal behaviors, i.e., cases with n sufficiently different from 1.

A similar continuous histogram of the peakedness parameter, ν, of the stretched exponential fits is shown in Figure 8. We note that ν, in general, is less than 1 and that the distribution peaks at approximately 0.75, i.e., almost all fitted pulse decays are *stretched* exponentials, rather than compressed ones. Here the two cases that were not constrained by the power law function, i.e., triggers 973 and 1121, are seen at $\nu = 1.26$ and $\nu = 1.0$.

The photon fluence associated with equation (10) when n differs from 1 becomes

$$\Phi(t) = \frac{N_0 \tau}{n-1} \left\{ 1 - (1 + t/\tau)^{-(n-1)} \right\}, \quad n \neq 1. \tag{11}$$

Fits of this function to the fluence data are presented in Figure (8) and the parameters obtained are shown in Table 7. The n value were fixed to the value obtained from the light curve fits of equation (10). The evolution of the fluence associated with the stretched exponential decay of the photon flux, $N(t)$, (eq. [1]) is given in an Appendix and was not used in the analysis.

To complete all aspects of the spectral/temporal evolution of the pulses in the sample, the temporal evolution of the peak energy, $E_{\rm pk}(t)$, according to equation (7) with the exponent, δ_* was studied. The results are presented in Figure (8) and the parameters obtained in Table 2. The exponent δ_* differs from δ when n is not equal to 1 in equation

(10). The time constant, τ, was frozen in these fits to the value obtained from the fits of equation (10) to the light curve. In Figure 8, a continuous histogram of the δ_*-values from the fits to $E_{\rm pk}(t)$ (eq. [7]) is shown. There are no obviously preferred values of δ_*.

5. Analytical Description of Generalized Pulse Decay Behaviors

As discussed in the Introduction, we will use the light curve, $N(t)$, as the point of departure for our analysis. In § 4, we found that the power law function, equation (10), is a better description of the pulse decays than equation (1). From now on, we assume that pulse decays can be described as power law decays.

Therefore we consider that the pulse decay follows equation (10), for a power law index, n, different from the previously studied standard case, $n = 1$, in RS00. The associated fluence is given by equation (11), which, for n larger than 1, converges to the asymptotic value $f_0 \equiv N_0\tau/(n-1)$.

Now, we consider two different alternatives. First, for GRB pulse light curves whose decays follow equation (10), and for which the HFC $E_{\rm pk}(\Phi)$ is an exponential given by equation (5), the HIC $E_{\rm pk}(N)$ will follow

$$E_{\rm pk}(N) = E_{\rm pk,0} \exp\left\{\frac{f_0}{\Phi_0}\left[\left(\frac{N}{N_0}\right)^{(n-1)/n} - 1\right]\right\}, \quad n \neq 1. \tag{12}$$

Note that f_0/Φ_0 is a dimensionless constant. When $\ln(N_0/N) \ll 2n/|n-1|$ the HIC in equation (12) approaches a power law with the exponent δ/n, which becomes identical to the original power law HIC in equation (4), as n tends to 1. The difference between the different HIC behaviors is best seen at the end of the decay of the pulse.

On the other hand, if the HIC $E_{\rm pk}(N)$ actually is a power law given by equation (4), then the HFC $E_{\rm pk}(\Phi)$ follows

$$E_{\rm pk}(\Phi) = E_{\rm pk,0}\left(1 - \frac{\Phi}{f_0}\right)^{n\delta/(n-1)}, \qquad n \neq 1, \tag{13}$$

which behaves similarly to equation (5) when $\Phi \ll f_0$, and becomes identical to that equation, if, in addition, n tends to 1. At the asymptotic value of $\Phi = f_0$, the peak energy has converged to zero.

The time evolution of $E_{\rm pk}(t)$ for the two cases is readily obtained by inserting $N(t)$, from equation (10), into equation (12), and by inserting $\Phi(t)$ (eq.[11]) into equation (13).

The two resulting time behaviors are

$$E_{\rm pk}(t) = E_{\rm pk,0} \exp\left\{\frac{f_0}{\Phi_0}\left[(1+t/\tau)^{-(n-1)} - 1\right]\right\}, \tag{14}$$

and

$$E_{\rm pk}(t) = E_{\rm pk,0}(1+t/\tau)^{-\delta_*}, \tag{15}$$

with $\delta_* \equiv n\delta$.

In an Appendix, we consider for completeness the stretched exponential pulse shape (eq. [1]), and its two corresponding correlations, the HIC $E_{\rm pk}(N)$ and the HFC $E_{\rm pk}(\Phi)$, respectively.

6. Three Complete Spectral/Temporal Pictures

Assuming that the decay phase of a pulse behaves as the power law function in equation (10), the whole spectral/temporal description will be complete according to RS00 for $n = 1$ and to §5 above for $n \neq 1$. Here, we consider three different cases, the one discussed in RS00 and § 2.3, and the two alternatives discussed in § 5:

i) The two correlations given by a power law HIC $E_{\rm pk}(N)$ (eq. [4]) and an exponential HFC $E_{\rm pk}(\Phi)$ (eq. [5]) are fitted to the data. Consequently the power law pulse decay has the index $n = 1$. In Table 4, we present the results, i.e., fitting the power law HIC $E_{\rm pk}(N)$ (eq. [4]) gives the parameters, $E_{\rm pk,0}$ and δ, and fitting the exponential HFC $E_{\rm pk}(\Phi)$ (eq. [5]) gives the parameters, $E_{\rm pk,0}$ and Φ_0. For the HIC fit, N_0, was frozen to the values in Table 2.

ii) The pulse decay is fitted as a power law of index n, the exponential HFC $E_{\rm pk}(\Phi)$ (eq. [5]) is assumed to be valid, and a fit is made to the generalized HIC $E_{\rm pk}(N)$ of § 5 (eq. [12]). Parameters for the exponential HFC $E_{\rm pk}(\Phi)$ can be found in Table 4. In Table 5, we present the fitting parameters of the generalized HIC $E_{\rm pk}(N)$ (eq. [12]), i.e., $E_{\rm pk,0}$ and f_0/Φ_0. N_0 and n were frozen to the values in Table 2.

iii) The pulse decay is fitted as a power law of index n, the power law HIC $E_{\rm pk}(N)$ (eq. [4]) is assumed to be valid, and a fit is made to a generalized HFC $E_{\rm pk}(\Phi)$ of § 5 (eq. [13]). Parameters for the power law HIC $E_{\rm pk}(N)$ can be found in Table 4. In Table 5, we present the fitting parameters of the generalized HFC $E_{\rm pk}(\Phi)$ (eq. [13]), i.e., $E_{\rm pk,0}$ and δ. $f_0 \equiv N_0\tau/(n-1)$ in equation (13) is frozen and calculated using N_0, τ, and n from Table 2.

The quality of the fits can be judged from the reduced χ^2 values in the Tables. The reason we chose to freeze N_0, τ, and n was to have a consistency with the light curve fittings in Table 2 and as these parameters often could not be constrained if they were free to vary.

The results are also presented in Figures 8. Here, the first panel in every horizontal strip shows the DISCSC data (all four energy channels are used) and indicates the time interval studied (also see Table 1). The second panel shows the light curve with the LAD HERB data in the chosen time binning. In some cases bins beyond the interval used for the statistical analysis is shown and indicated in grey (cf. Table 1 and §4). The best fit is indicated with a solid curve (see Table 2). The two right-hand panels, show the correlations, the HIC $E_{\rm pk}(N)$ in panel 3 and the HFC $E_{\rm pk}(\Phi)$ in panel 4. Case (i) (i.e., $n = 1$) is represented by the solid line in panel 3 (the power law HIC $E_{\rm pk}(N)$) and the dashed line in panel 4 (the exponential HFC $E_{\rm pk}(\Phi)$). Case (ii) is represented by the dashed curves in the two panels, the generalized HIC $E_{\rm pk}(N)$ in panel 3 and the exponential HFC $E_{\rm pk}(\Phi)$ in panel 4. Finally, case (iii) is represented by the solid curves in the two panels, the power law HIC $E_{\rm pk}(N)$ in panel 3 and the generalized HFC $E_{\rm pk}(\Phi)$ in panel 4.

First, note the self-consistent behavior of the about 10 cases with $n \sim 1$ as was already outlined and studied in RS00. For such cases, the power law HIC $E_{\rm pk}(N)$ and the exponential HFC $E_{\rm pk}(\Phi)$ are valid simultaneously.

For the 11 pulse decays with n larger than 2, it could be the case that both the HIC $E_{\rm pk}(N)$ and the HFC $E_{\rm pk}(\Phi)$ are described by completely new functions. However, it could also be the case that only one, either the HIC $E_{\rm pk}(N)$ or the HFC $E_{\rm pk}(\Phi)$, is different, leaving the other correlation valid independent of the shape of the light curve (i.e., of n). In the results (Tables 4 and 5), there is such a correspondence, i.e., if the power law HIC $E_{\rm pk}(N)$ in Table 4 gives a better fit than the generalized HIC $E_{\rm pk}(N)$ in Table 5, then the generalized HFC $E_{\rm pk}(\Phi)$ in Table 5 is a better fit than the exponential HFC $E_{\rm pk}(\Phi)$ in Table 4 and vice versa. About half the cases point to the power law HIC $E_{\rm pk}(N)$ being valid independent of the shape of the light curve, while the other half suggests the exponential HFC $E_{\rm pk}(\Phi)$ to be the one that is valid. Unfortunately, the correlations are not of sufficiently quality to distinctly favor one set or the other, which is also seen in the two right-hand panels in Figure 8.

To check the significance of these results and to find which pulses can with some confidence be said to favor either a power law HIC or an exponential HFC, we study the following. For every pulse, the pair with the best fits, i.e., either a power law HIC plus a generalized HFC or a generalized HIC plus an exponential HFC, are considered and we reanalyze the generalized correlation (given by either equation [12] or [13]) by letting the parameter n also be free to vary. The results are presented in Table 6. In 6 out of the 11 cases, n is constrained. Four out of these give n-values that are the same to within the errors as the values obtained from fitting the light curve (Table 2). For these cases, the spectral/temporal behavior is consistent and constrained. In the last two cases for which n

is constrained, the errors in the n-values are, however, so large that no certain conclusion can be drawn.

The four cases (triggers 1625, 3492, 3765, and 5567) for which the correlations are good enough to be able to draw any conclusions are all consistent with case (iii) above, i.e., a power law HIC $E_{\rm pk}(N)$ (according to eq. [4]) and a generalized HFC $E_{\rm pk}(\Phi)$ (according to eq. [13]). These cases are marked with an asterisk in Figure 8 and the resulting generalized HFCs from having the n-parameter free to vary are also indicated in Figure 8 by long-dashed curves in the right-hand panel for the four triggers. The HICs for these four cases are also found to be described by power laws in the study of Borgonovo & Ryde (2001) and they are thus expected to have an HFC $E_{\rm pk}(\Phi)$ differing from an exponential.

7. Discussion

7.1. Comments on the Analysis

In parentheses in Table 1, the total number of bins which were studied is given. The extra time bins are not included in the statistical analysis but are nonetheless included in Figure 8 in grey. In these cases, the light curves show details which motivate their exclusion. This is especially seen in linear plots of the decay, i.e., when plotting the linear $N(t)^{-1/n}$. This is, for instance, seen for the pulse from trigger 6630 in Figure 1 in RS00. The inclusion of these data points often leads to a drastic increase in the error of the n-parameter with, albeit, n still being consistent with the n from fitting only the earlier decay phase.

Specifically, for trigger 3492, the choice of the fitting time interval is motivated by its appearance in a $1/N(t)$-plot, see Figure 8. The extra bump at 8 seconds could be an additional pulse. Fitting the whole interval out to 8.5 s with the power law function (eq.[10]) gives a very high, $\chi^2 \sim 30$.

Furthermore, for pulse 2083:2, only 8 out of the 11 analyzed time bins are used in our study. The reason for this is the low values of the measured peak energy, ~ 20 keV, which is at or below the actual detector energy window, and should thus not be included in the statistical analysis.

The strange behavior of trigger 3954 could be due to a track jump similar to the ones discussed by Borgonovo & Ryde (2001).

The light curve of trigger 3345 before and after the HERB data is very uneven and complicated. This makes the background estimate very difficult and affects the detailed analysis and thus this case should be treated with some caution. We, therefore, choose a

$S/N = 45$. Note that Borgonovo & Ryde (2001) use a higher time resolution (and a lower S/N) and identify detailed structure in the HIC.

Finally, trigger 7527 was chosen to be studied up to 12 s, for which the power law index of the photon flux decay was $n = 1.2 \pm 0.6$. Including the two last time bins, the index becomes undetermined, $n = 7 \pm 9$. Again there is a distinct shoulder in the light curve around 12 s, which can be interpreted as being a result of a change of the radiative regime and, if included, results in the badly determined parameter n.

By requiring pulse decays to have several time bins with $S/N = 30 - 45$ automatic leads to a biasing against short pulses with fast decays, and it should be noted that the conclusions of our work are only valid for bright and long pulses. The behavior of short pulses in long bursts and short pulses in short bursts should be studied to find out whether the spectral/temporal behavior differs in any manner. For this, more sensitive detectors are needed.

7.2. Stretched Exponential

For our study of the decay shape of pulses, we have mainly been using the power law decay function. However, we have also fitted the stretched exponential function. We found that the distribution of the peakedness parameter of the stretched exponential function peaks at $\nu \sim 0.7$, see Fig. (8). This is in contrast to the results of Norris et al. (1996), who found ν to lie predominantly between 1 and 2. Note, however, that there are several important differences between their work and ours. First of all, we study the pulses in photon fluxes over the whole energy band of the BATSE detector, while Norris et al. studied the photon count rate in the four individual channels. The pulse shape over the whole spectral range is the sum of the pulse shapes for the individual channels. We also only study long pulses. Moreover, we study exclusively the decay phase of the pulses, while the Norris et al. study includes also the rise phase using the same value for ν. The peakedness parameter thus describes the sharpness of the peak. Finally, our criterion of sufficient S/N in at least 8 time bins for a pulse to be selected probably causes a bias against high-ν pulses, as these decay too rapidly to satisfy the criterion.

Note that the stretched exponential function was invented and used mainly as a parameterization and description of the light curve, and especially for that of the *entire* pulse. We are searching for the self-consistent description of the total spectral and temporal behavior and we have shown that the power law function is valid for most cases. It does not merely serve as a multi-parameter function to fit the light curves, but it is a prediction

based on the known evolution described by the two correlations.

7.3. Underlying Physical Mechanisms

A general consideration for a radiative pulse, and also the motivation for concentrating on the decay phase, is that the rise phase describes the energization of the emitting plasma and the size of the activated region, while the decay phase provides information on the cooling. The different aspects of the behavior during the decay phase of a pulse, demonstrated in this paper, reflects the underlying physics during this cooling phase. There is, unfortunately no straight-forward physical interpretation of these relations. There are probably several different processes at action and a competition between these finally decides the details in the spectral evolution.

In the standard fireball internal/external shock model every individual pulse is identified with a separate emission episode, as a result of a collision between two shells in the relativistic outflow (or as an interaction with the circum-burst interstellar medium) in which the ordered kinetic energy of the outflow is transformed into random energy of the leptons which radiate. The main radiative processes considered for the BATSE band radiation is synchrotron emission or reprocessing of a low energy synchrotron spectrum by inverse Compton scattering. The main motivation for this is due to the efficiency of these processes and the natural role they play in relativistic shocks. However, the radiative cooling time scales for these processes are, in general, very short (see for instance Ghisellini, Celotti, & Lazzati 2000) and therefore a direct interpretation of the pulses as a result of an impulsive heating with a subsequent decay is difficult. Rather a continuous acceleration of the leptons, competing with the radiative cooling, could be invoked to explain the time scales of the long pulses studied here. Thus the light curve probably reflects the change in plasma properties, such as the lepton energy distribution. The actual acceleration process which takes place in the shocks is not well understood and is mainly assumed to produce a power law distribution of leptons. The observed spectral and temporal signatures during pulse decays give insights into these processes. Ryde, Lloyd, & Petrosian (in preparation) study the synchrotron emission and the associated lepton distribution needed to reproduce these signatures, especially the HIC $E_{\rm pk}(N)$ since it seems to be one of the fundamental relations.

As an alternative radiation mechanism, Liang (1997) and Liang et al. (1999) have explored a thermal Comptonization model based on the observations of the HFC. An emitting system that reproduces the observations that the hardness of the instantaneous spectra decays exponentially with photon fluence is the following. Assume a confined

plasma that is subject to an impulsive energy release, heating the gas. Assume further that there is a constant supply of soft photons that cools the hot electron gas in the plasma, giving rise to thermal radiation and the radiated luminosity. With a thermal radiation process, e.g., saturated Comptonization, the averaged photon energy will correspond to the electron temperature. The cooling of the electron gas then gives rise to the evolution of the peak of the photon spectrum. The change of the total energy of the cloud, i.e., the luminosity radiated away, will therefore be proportional to the change in photon energy, if the number of electrons is constant. This is what is described by the power-law HFC. Equation (5) gives that the change of the photon energy will be proportional to the emitted flux: $-dE_{\rm pk}/dt \propto N(t)E_{\rm pk}(t) \propto F$. Note that any thermal process will be able to reproduce this relation. Also, as mentioned above, there is a continuous heating, for instance from dissipation of energy through shocks which complicates the picture.

Moreover, kinematical and relativistic effects should also be considered. The dynamics of the actual shell crossing will be affected by the shell widths and the relative sizes of the Lorentz factors and densities of the two shells and could contribute to the dispersion in the observed behaviors. And as the radiation is emitted from a spherical symmetric surface expanding at a relativistic speed, with Lorentz factors of $10^2 - 10^3$, light travel effects could become as important as other effects. This will smear out any direct physical information in the spectra; see, for instance, Cen (1999). If this effect is indeed dominating, the pulse shape will no longer reflect the intrinsic temporal profile. Ryde et al. (in preparation) is investigating this issue in detail and comparing it to the observational results above.

Finally, as emphasized by RS00 and in this paper, the different aspects of the spectral and temporal evolution are intimately linked to each other. It is therefore not enough to explain only one aspect, such as the light curve decoupled from the spectral behavior. The full spectral/temporal description should be tested for in any successful model attempting to describe the prompt GRB emission.

8. Conclusions

We have presented and shown, through the two empirical correlations, the HFC $E_{\rm pk}(\Phi)$ and the HIC $E_{\rm pk}(N)$, how we can characterize the variety of the decays of long, bright GRB pulses. Since the light curve, $N(t)$, is the best determined with relatively small errors (as compared to the correlations, or $E_{\rm pk}[t]$) and gives the strongest constraint to the fits, we start our exploration from the variety of shapes of the light curve. This leads us to find alternative $E_{\rm pk}(N)$ and $E_{\rm pk}(\Phi)$ behaviors.

A bimodality could be present, in that there are two preferred values of the index of the power-law light-curve, namely $n \sim 1$ and $n \sim 3$, with the sample divided into approximately two equally large sets by $n \sim 2$. For the large n cases, we could identify 4 cases for which the spectral/temporal behavior, i.e., the correlations, was constrained (even if n was free). These cases suggest that the power law HIC $E_{\rm pk}(N)$ is valid independent of the shape of the light curve, i.e., there is always the same power law correlation between the hardness and the intensity. The HFC $E_{\rm pk}(\Phi)$, on the other hand, is different for different light curve behaviors according to equation (13), since the fluence is the time integral of the instantaneous flux.

The important relations for a GRB pulse decay are, subsequently, the power law HIC $E_{\rm pk}(N)$ and the light curve, $N(t)$. However, it must be noted that this result should be tested on a larger sample of well determined HICs and HFCs to be able to clearly confirm our conclusions. A catalog of strong GRB pulses and their behaviors is in preparation.

We are grateful to the GROSSC at Goddard Space Flight Center for help during our work with the BATSE data and the WINGSPAN program. This research made use of data obtained through the HEASARC Online Service provided by NASA/GSFC. Furthermore, we would like to thank Robert Preece, Luis Borgonovo, Andrei Beloborodov, and Juri Poutanen for various help. We also thank the referee, Jay Norris, for valuable comments. We acknowledge support from the Gustaf and Ellen Kobb's Stipend Fund at Stockholm University, the Swedish National Space Board and the Swedish Natural Science Research Council (NFR).

Appendix: The Stretched Exponential Light Curve and its Corresponding Correlations

For completeness and as the stretched exponential of equation (1) is the most commonly used when fitting light curves of pulses, we also present a full analytical treatment of its relation to the HIC $E_{\rm pk}(N)$ and the HFC $E_{\rm pk}(\Phi)$.

First, we study what the HIC $E_{\rm pk}(N)$ would be if the decay phase of the light curve were a stretched exponential given by equation (1) with $t_{\rm max} = 0$. Note that the time constant, $\tau_{\rm d}$, is different from τ. The range of ν of interest from Figure 2 is 0.5 - 2.

The case $\nu = 0.5$ gives

$$\Phi(t) = 2N_0\tau_{\rm d}\left(1 - (1 + \sqrt{t/t_d})e^{-\sqrt{t/t_d}}\right) \tag{16}$$

. Now, assuming an exponential HFC $E_{\rm pk}(\Phi)$ (eq. [5]) to be valid for the pulse decay gives the following HIC

$$E_{\rm pk}(N) = E_{\rm pk,0} \exp\left(-\frac{2N_0\tau_{\rm d}}{\Phi_0}\left[1 - \frac{N(t)}{N_0}\left(1 - \ln\frac{N}{N_0}\right)\right]\right). \tag{17}$$

For a pure exponential pulse decay (i.e., $\nu = 1$), we get

$$\Phi(t) = N_0\tau_{\rm d}\left(1 - e^{-t/\tau_{\rm d}}\right) = N_0\tau_{\rm d}\left(1 - \frac{N(t)}{N_0}\right), \tag{18}$$

which for an exponential HFC $E_{\rm pk}(\Phi)$ gives the HIC

$$E_{\rm pk}(N) = E_{\rm pk,0} \exp\left[-\frac{N_0\tau_{\rm d}}{\Phi_0}\left(1 - \frac{N(t)}{N_0}\right)\right]. \tag{19}$$

As N approaches N_0 this is the same relation as equation (4) with $N_0\tau_{\rm d}/\Phi_0 = \delta$. Correspondingly, $t/\tau_{\rm d}$ tends to 0. For $N \ll N_0$, the HICs differ and can thus be tested for in the observations.

For a Gaussian pulse profile ($\nu = 2$) we get

$$\Phi(t) = N_0\tau_{\rm d}(\sqrt{\pi}/2){\rm erf}(t/\tau_{\rm d}), \tag{20}$$

where ${\rm erf}(x)$ is the Gauss error function. Combined with the exponential HFC $E_{\rm pk}(\Phi)$, the HIC $E_{\rm pk}(N)$ becomes

$$E_{\rm pk}(N) = E_{\rm pk,0} \exp\left[\frac{\sqrt{\pi}}{2}\frac{N_0\tau_{\rm d}}{\Phi_0}{\rm erf}(\sqrt{-\ln N/N_0})\right]. \tag{21}$$

Thus using a stretched exponential describing the light curve will, of necessity, make the HIC $E_{\rm pk}(N)$ more complicated. Instead of a power law relation between the hardness and the intensity, the HIC $E_{\rm pk}(N)$ becomes complicated exponential relations.

We now assume that the power law HIC $E_{\rm pk}(N)$ (eq. [4]) is valid instead of the exponential HFC $E_{\rm pk}(\Phi)$. An analytical solution can only be found for an exponential light curve ($\nu = 1$). Solving for N/N_0 in equation (18) and inserting in equation (4) gives

$$E_{\rm pk} = E_{\rm pk,0}\left(1 - \frac{\Phi(t)}{N_0\tau_{\rm d}}\right)^{\delta}. \tag{22}$$

As $\Phi(t)$ approaches 0, this is the same relation as equation (5) with $N_0\tau_{\rm d}/\Phi_0 = \delta$. Correspondingly, $t/\tau_{\rm d}$ tends to 0. For $\Phi \gg \Phi_0$, the HFCs differ and can thus be tested for in the observations.

REFERENCES

Band, D., et al. 1993, ApJ, 413, 281

Borgonovo, L., & Ryde, F. 2001, ApJ, 548, 770

Cen, R. 1999, ApJ, 517, L113

Crider, A., Liang, E. P., & Preece, R. D. 1998, in AIP Conf. Proc. 428, Gamma-Ray Bursts, 4th Huntsville Symposium., ed. C. A. Meegan, R. D. Preece, T. M. Koshut (New York: AIP), 63

Fishman, G. J., et al. 1989, in Proc. of the GRO Science Workshop, ed. W. N. Johnson, 2

Fishman, G. J., et al. 1994, ApJS, 92, 229

Ford, L. A., et al. 1995, ApJ, 439, 307

Ghisellini, G., Celotti, A, & Lazzati, D. 2000, MNRAS 313, L1

Giblin, T. W., van Paradijs, J., Kouveliotou, C., Connaughton, V., Wijers, R. A. M. J., Briggs, M. S., Preece, R. D., & Fishman, G. J. 1999, ApJ, 524, L47

Golenetskii, S. V., Mazets, E. P., Aptekar, R. L., & Ilyinskii, V. N. 1983, Nature, 306, 451

Kargatis V. E., Liang, E. P., Hurley, K. C., Barat, C., Eveno, E., & Niel, M. 1994, ApJ, 422, 260

Kargatis, V. E., et al. 1995, A&SS, 231, 177

Lee, A., Bloom, E., & Scargle, J. 1998, in AIP Conf. Proc. 428, Gamma-ray Bursts, 4th Huntsville Symposium, ed. C. A. Meegan, R. D. Preece & T. M. Koshut (New York: AIP), 261

Liang, E. P. 1997, ApJ, 491, L15

Liang, E. P., & Kargatis, V. E. 1996, Nature, 381, 495

Liang, E. P., Kusunose, M., Smith, I. A., & Crider, A. 1997, ApJ, 479, L35

Norris, J. P., Nemiroff, R. J., Bonnell, J. T., Scargle, J. D., Kouveliotou, C., Paciesas, W. S., Meegan, C.A., & Fishman, G. J. 1996, ApJ, 459, 393

Pendleton, G. N., et al. 1995, NIMSA, 364, 567

Preece, R. D., Briggs, M. S., Mallozzi, R. S., & Brock, M. N. 1996, WINGSPAN v 4.4 manual

Preece, R. D., Pendleton, G. N., Briggs, M. S., Mallozzi, R. S., Paciesas, W. S., Band, D. L., Matteson, J. L., & Meegan, C. A. 1998, ApJ, 496, 849

Press, W. H., Teukolsky, S. A., Vetterling, W. T., & Flannery, B. P. 1992, Numerical Recipes in Fortran (2d ed.; Cambridge: Cambridge Univ. Press)

Ryde, F. 1999, in Gamma-Ray Bursts: The First Three Minutes, ed. J. Poutanen, & R. Svensson, ASP Conf. Ser. 190 (San Francisco: ASP), 103

Ryde, F., & Svensson, R. 1999, ApJ, 512, 693

Ryde, F., & Svensson, R. 2000, ApJ, 529, L13 (RS00)

Ryde, F., & Svensson, R. 2001, in the proceedings of 'Gamma-Ray Burst in the Afterglow Era – 2nd. Workshop, in press

Schaefer, B. E., & Dyson, S. E. 1996, in AIP Conf. Proc. 384, Gamma-ray Bursts, 3rd Huntsville Symposium, ed. C. Kouveliotou, M. F. Briggs & G. J. Fishman (New York: AIP), 96

Scargle, J. D. 1998, ApJ, 504, 405

Stern, B. E. 1999, in ASP Conf. Series Vol. 161, High Energy Processes in Accreting Black Holes, ed. J. Poutanen & R. Svensson (San Francisco: ASP), 277

Stern, B., & Svensson, R. 1996, ApJ, 469, L109

Table 1: The Sample of 25 Pulse Decays

Burst	Trigger	LAD	$n_{\rm bins}$[a]	Time interval[b]
GRB910627	451	4	8	5.57-14.144
GRB910897	647	0	7(8)	14.46-19.39(20.35)
GRB910927	829	4	9(10)	6.53-14.85(20.16)
GRB911031	973	3	15	3.07-12.42
GRB911118	1085	4	13	9.22-17.73
GRB911126	1121	4	8	21.82-24.13
GRB911202	1141:1	7	10	3.90-6.78
	1141:2	7	10(12)	9.28-17.86(25.15)
GRB920525	1625	4	10(11)	4.93-7.55(8.96)
GRB920623	1663	4	10	16.96-27.58
GRB921207	2083:1	0	21	1.09-5.38
	2083:2	0	8(11)	8.77-14.34(30.40)
GRB930201	2156	1	11	14.85-21.76
GRB940410	2919	6	13(14)	0.32-7.81(12.42)
GRB940623	3042	1	13	8.00-19.20
GRB950104	3345	1	7	5.70-20.16
GRB950403	3492	5	10(16)	5.25-6.98(11.5)
GRB950624	3648	3	10(11)	41.02-50.50(56.90)
GRB950818	3765	1	10(11)	66.37-70.91(73.28)
GRB951016	3870	5	13	0.64-5.44
GRB951213	3954	2	15	1.15-11.90
GRB960807	5567	0	8	12.10-17.79
GRB970223	6100	6	16(17)	8.32-16.06(18.37)
GRB980306	6630	3	7(8)	2.24-5.70(7.74)
GRB990424	7527	7	10(12)	6.40-11.97(17.15)

[a] $n_{\rm bins}$ is the number of time bins studied in the pulse decay. [b] The time interval during which the decay was studied in detail in seconds since the trigger.

Table 2: Power Law Fits of the Intensity and Peak Energy of the 25 Pulse Decays

	$N(t)$[a]				$E_{\rm pk}(t)$[b]		
Trigger	N_0 ($\rm cm^{-2}$ $\rm s^{-1}$)	τ (s)	n	χ^2_ν/d.o.f	$E_{\rm pk,0}$(keV)	δ_*	χ^2_ν/d.o.f
451	29.4 ± 0.6	4.7 ± 0.8	3.2 ± 0.4	3.97	91 ± 8	1.3 ± 0.4	1.95
647	6.77 ± 0.20	4.2 ± 2.6	1.2 ± 0.5	0.46	235 ± 18	0.76 ± 0.25	1.12
829	10.1 ± 0.3	2.8 ± 0.8	1.06 ± 0.17	1.2	109 ± 3	0.27 ± 0.04	1.99
973	-	-	-	-	-	-	-
1085	25.6 ± 0.4	22 ± 11	5.4 ± 2.4	2.4	119.0 ± 1.6	3.35 ± 0.11	0.55
1121	-	-	-	-	-	-	-
1141:1	18.5 ± 0.5	2 ± 3	0.3 ± 0.3	2.38	380 ± 55	0.29 ± 0.26	1.19
1141:2	26.9 ± 1.3	0.82 ± 0.24	0.71 ± 0.08	2.58	410 ± 105	0.66 ± 0.16	6.30
1625	63 ± 3	2.1 ± 0.8	2.7 ± 0.8	6.42	800 ± 80	1.7 ± 0.3	1.22
1663	48 ± 5	0.37 ± 0.11	1.00 ± 0.08	11.68	825 ± 70	0.88 ± 0.07	2.08
2083:1	98 ± 5	0.63 ± 0.13	1.03 ± 0.09	9.17	466 ± 14	0.928 ± 0.024	1.79
2083:2	31.5 ± 0.6	13 ± 7	5.3 ± 2.5	1.94	109.0 ± 2.1	3.51 ± 0.16	0.80
2156	29.5 ± 0.8	7 ± 3	3.4 ± 1.1	2.07	380 ± 60	2.5 ± 0.5	2.81
2919	12.7 ± 0.3	8.6 ± 2.9	3.2 ± 0.9	0.89	197 ± 40	2.2 ± 1.0	1.31
3042	13.6 ± 0.6	1.14 ± 0.26	1.10 ± 0.11	2.62	375 ± 55	0.65 ± 0.10	0.63
3345	13.8 ± 0.6	1.2 ± 0.3	0.97 ± 0.08	1.58	132 ± 17	0.35 ± 0.12	0.90
3492	150 ± 6	0.86 ± 0.19	2.3 ± 0.3	4.37	530 ± 55	1.13 ± 0.20	1.95
3648	10.2 ± 0.4	2.5 ± 0.7	1.18 ± 0.18	1.73	284 ± 21	1.24 ± 0.10	1.81
3765	48.3 ± 1.1	3.5 ± 0.8	3.0 ± 0.5	2.04	345 ± 21	1.29 ± 0.13	1.72
3870	36.5 ± 1.1	1.7 ± 0.3	1.64 ± 0.19	2.12	59 ± 7	0.14 ± 0.13	1.07
3954	19.7 ± 0.6	4.5 ± 0.6	2.7 ± 0.4	1.96	105 ± 25	0.1 ± 0.4	2.61
5567	47.6 ± 2.1	1.8 ± 0.4	2.7 ± 0.4	6.45	515 ± 16	0.73 ± 0.09	0.13
6100	40.4 ± 1.0	4.5 ± 0.8	2.9 ± 0.4	3.11	500 ± 50	1.80 ± 0.25	2.26
6630	23.2 ± 0.8	1.5 ± 0.6	1.10 ± 0.25	1.94	242 ± 5	1.20 ± 0.03	0.42
7527	21.0 ± 1.5	2.5 ± 2.0	1.2 ± 0.6	9.31	420 ± 40	0.83 ± 0.14	1.75

[a]Parameters for the fits to equation (10). [b]Parameters for the fits to equaton (7) with the exponent δ_*. δ_* differs from δ when $n \neq 1$.

Table 3: Stretched Exponential Fits to the Intensity of the 25 Pulse Decays

	$N(t)$[a]			
Trigger	$N_0(\mathrm{cm}^{-2}\mathrm{s}^{-1})$	τ_d (s)	ν	χ^2/d.o.f
451	31.3 ± 2.5	1.62 ± 0.21	0.77 ± 0.07	6.20
647	7.0 ± 0.4	5.3 ± 0.3	0.75 ± 0.12	0.57
829	9.9 ± 0.6	4.5 ± 0.5	0.80 ± 0.08	4.1
973	12.40 ± 0.21	5.77 ± 0.11	1.26 ± 0.05	1.0
1085	26.2 ± 0.6	4.42 ± 0.14	0.89 ± 0.04	2.21
1121	25.3 ± 1.0	2.36 ± 0.10	1.01 ± 0.12	1.76
1141:1	18.8 ± 0.9	15 ± 8	0.7 ± 0.3	2.39
1141:2	40 ± 8	1.1 ± 0.6	0.37 ± 0.06	3.21
1625	69 ± 5	0.84 ± 0.10	0.74 ± 0.07	6.36
1663	200 ± 150	0.01 ± 0.03	0.24 ± 0.07	19.2
2083:1	130 ± 15	0.61 ± 0.15	0.46 ± 0.04	10.4
2083:2	32.0 ± 1.1	2.8 ± 0.13	0.91 ± 0.06	2.61
2156	30.3 ± 1.5	2.41 ± 0.18	0.85 ± 0.07	3.11
2919	13.3 ± 0.4	3.02 ± 0.15	0.81 ± 0.04	0.85
3042	18.8 ± 2.4	0.91 ± 0.28	0.45 ± 0.05	2.92
3345	19.1 ± 2.2	1.2 ± 0.3	0.43 ± 0.04	1.79
3492	183 ± 20	0.34 ± 0.06	0.65 ± 0.06	8.30
3648	11.5 ± 1.0	2.8 ± 0.5	0.59 ± 0.07	2.78
3765	52.1 ± 1.7	1.27 ± 0.07	0.76 ± 0.03	1.79
3870	42.1 ± 1.6	1.15 ± 0.08	0.62 ± 0.03	3.12
3954	21.5 ± 1.2	1.80 ± 0.17	0.72 ± 0.05	2.78
5567	56 ± 7	0.64 ± 0.14	0.67 ± 0.07	17.4
6100	43.4 ± 2.2	1.71 ± 0.14	0.75 ± 0.04	5.91
6630	25.2 ± 2.0	2.0 ± 0.3	0.65 ± 0.09	2.88
7527	23 ± 3	2.9 ± 0.7	0.66 ± 0.16	10.77

[a]Parameters for the fits to equation (1).

Table 4: Fits of the Power-law HIC $E_{\rm pk}(N)$ and the Exponential HFC $E_{\rm pk}(\Phi)$ to 23 Pulse Decays.

	HIC $E_{\rm pk}(N)$[a]			HFC $E_{\rm pk}(\Phi)$[b]		
Trigger	$E_{\rm pk,0}$ (keV)	δ	χ^2/d.o.f.	$E_{\rm pk,0}$ (keV)	Φ_0	χ^2/d.o.f.
451	92 ± 8	0.42 ± 0.13	1.75	98 ± 8	61 ± 16	1.42
647	232 ± 19	0.60 ± 0.22	1.33	260 ± 28	36 ± 12	1.14
829	109 ± 3	0.26 ± 0.03	1.58	109 ± 3	99 ± 13	1.98
1085	118.8 ± 1.5	0.649 ± 0.019	0.50	129 ± 3	98 ± 4	1.14
1141:1	381 ± 50	0.9 ± 0.7	1.14	385 ± 60	175 ± 155	1.19
1141:2	405 ± 105	0.93 ± 0.23	6.55	375 ± 85	50 ± 11	5.70
1625	640 ± 50	0.59 ± 0.07	1.12	925 ± 120	42 ± 7	1.57
1663	815 ± 70	0.89 ± 0.07	2.05	780 ± 65	20.3 ± 1.6	2.29
2083:1	460 ± 13	0.885 ± 0.020	1.42	470 ± 14	64.8 ± 1.6	1.70
2083:2	108 ± 3	0.65 ± 0.04	1.33	116.7 ± 1.7	75.1 ± 2.2	0.35
2156	389 ± 55	0.74 ± 0.14	2.48	490 ± 70	42 ± 6	1.81
2919	205 ± 40	0.7 ± 0.3	1.26	220 ± 50	31 ± 12	1.25
3042	350 ± 55	0.55 ± 0.10	0.78	390 ± 60	21 ± 3	0.61
3345	134 ± 16	0.36 ± 0.12	0.82	132 ± 16	48 ± 17	0.90
3492	535 ± 55	0.48 ± 0.08	1.83	565 ± 80	65 ± 14	2.85
3648	288 ± 20	1.06 ± 0.07	1.51	302 ± 20	17.3 ± 1.1	1.28
3765	347 ± 21	0.43 ± 0.04	1.63	390 ± 35	64 ± 8	2.66
3870	58 ± 7	0.08 ± 0.08	1.08	64 ± 9	195 ± 135	1.00
3954	100 ± 24	0.02 ± 0.14	2.62	125 ± 50	120 ± 170	2.55
5567	516 ± 17	0.27 ± 0.03	0.14	545 ± 35	59 ± 12	0.39
6100	500 ± 50	0.61 ± 0.08	2.18	595 ± 60	52 ± 6	1.94
6630	243 ± 6	1.09 ± 0.03	0.74	245 ± 6	28 ± 0.9	0.75
7527	427 ± 28	0.69 ± 0.09	1.10	425 ± 40	57 ± 10	1.85

[a]Fits of power law HIC $E_{\rm pk}(N)$ according to equation (4). N_0 is frozen to the values in Table 2.
[b]Fits of exponential HFC $E_{\rm pk}(\Phi)$ according to equation (5).

Table 5: Fits of Generalized HIC $E_{\rm pk}(N)$ and HFC $E_{\rm pk}(\Phi)$ for Different n to 23 Pulse Decays.

		HIC $E_{\rm pk}(N)$[a]			HFC $E_{\rm pk}(\Phi)$[b]		
Trigger	n	$E_{\rm pk,0}$ (keV)	f_0/Φ_0	χ^2/d.o.f.	$E_{\rm pk,0}$ (keV)	δ	χ^2/d.o.f.
451	3.19	100 ± 8	1.1 ± 0.3	1.20	92 ± 8	0.42 ± 0.13	1.77
647	1.16	233 ± 20	4.5 ± 1.7	1.35	257 ± 27	0.63 ± 0.21	1.13
829	1.06	110 ± 3	4.7 ± 0.5	1.58	109 ± 3	0.26 ± 0.03	1.98
1085	5.43	128.7 ± 2.4	1.31 ± 0.05	0.86	118.9 ± 1.6	0.651 ± 0.020	0.57
1141:1	0.34	380 ± 45	-0.4 ± 0.3	1.14	390 ± 65	0.9 ± 0.8	1.19
1141:2	0.71	375 ± 85	-1.6 ± 0.4	6.03	405 ± 100	0.92 ± 0.22	6.30
1625	3.31	710 ± 90	1.7 ± 0.3	2.10	795 ± 75	0.64 ± 0.10	1.22
1663	1.00	815 ± 70	1330 ± 100	2.05	780 ± 70	0.88 ± 0.07	2.29
2083:1	1.03	466 ± 12	27.8 ± 0.6	1.33	463 ± 14	0.891 ± 0.023	1.77
2083:2	5.28	117.0 ± 1.9	1.31 ± 0.04	0.46	108.9 ± 2.0	0.67 ± 0.03	0.71
2156	3.43	490 ± 65	2.1 ± 0.3	1.70	385 ± 60	0.74 ± 0.16	2.75
2919	3.22	225 ± 50	1.7 ± 0.6	1.20	195 ± 40	0.7 ± 0.3	1.31
3042	1.10	370 ± 60	7.0 ± 1.2	0.75	375 ± 55	0.59 ± 0.09	0.63
3345	0.97	133 ± 16	-13 ± 4	0.83	133 ± 17	0.37 ± 0.13	0.89
3492	2.34	590 ± 85	1.5 ± 0.3	2.62	520 ± 55	0.48 ± 0.09	2.01
3648	1.18	303 ± 18	8.0 ± 0.5	1.11	285 ± 20	1.07 ± 0.08	1.68
3765	3.03	395 ± 35	1.32 ± 0.16	2.41	347 ± 22	0.44 ± 0.04	1.72
3870	1.64	63 ± 9	0.4 ± 0.3	1.02	59 ± 7	0.09 ± 0.08	1.07
3954	2.70	115 ± 45	0.2 ± 0.6	2.60	104 ± 26	0.04 ± 0.14	2.61
5567	2.70	555 ± 30	0.87 ± 0.15	0.32	518 ± 19	0.29 ± 0.04	0.17
6100	2.90	595 ± 60	1.84 ± 0.21	1.89	505 ± 50	0.63 ± 0.09	2.24
6630	1.10	246 ± 7	12.6 ± 0.5	0.99	242 ± 5	1.10 ± 0.03	0.47
7527	1.22	435 ± 30	4.2 ± 0.6	1.17	420 ± 35	0.68 ± 0.12	1.80

[a] Fits of HIC $E_{\rm pk}(N)$ according to generalized equation (12) assuming the existence of an exponential HFC $E_{\rm pk}(\Phi)$ (see equation [5] and Table 4) and using the n obtained by fitting the light curve, $N(t)$ (see Table 2). N_0 is frozen to the values in Table 2. [b] Fits of HFC $E_{\rm pk}(\Phi)$ according to generalized equation (13) assuming the existence of a power law HIC $E_{\rm pk}(N)$ (see equation [4] and Table 4) and using the n obtained by fitting the light curve, $N(t)$ (see Table 2). $f_0 \equiv N_0\tau/(n-1)$ is frozen and calculated using N_0, τ and n from Table 2.

Table 6: Fits of Generalized HIC $E_{\rm pk}(N)$ or HFC $E_{\rm pk}(\Phi)$ for the 11 High n Decays

Trigger	$n^{\rm a}$	$n^{\rm b}$	$E_{\rm pk,0}$ (keV)	f_0/Φ_0	δ	χ^2/d.o.f.	Correlation[c]
451	3.2 ± 0.4	N/C	-	-		-	HIC
1085	5.4 ± 2.4	N/C	-		-	-	HFC
1625	2.7 ± 0.8	3.25 ± 0.13	695 ± 75		0.30 ± 0.11	1.17	HFC
2083:2	5.3 ± 2.5	2.9 ± 1.6	115 ± 3	1.5 ± 0.3		0.48	HIC
2156	3.4 ± 1.1	N/C	-	-		-	HIC
2919	3.2 ± 0.9	N/C	-	-		-	HIC
3492	2.4 ± 0.3	2.68 ± 0.18	495 ± 55		0.29 ± 0.13	1.94	HFC
3765	3.0 ± 0.5	3.1 ± 0.4	340 ± 30		0.39 ± 0.18	1.95	HFC
3954	2.7 ± 0.4	N/C	-	-		-	HIC
5567	2.7 ± 0.4	2.98 ± 0.06	500 ± 15		0.19 ± 0.04	0.130	HFC
6100	2.9 ± 0.4	2.2 ± 1.9	580 ± 85	2.0 ± 0.8		2.02	HIC

[a] n from Table 2. [b] n is free to vary. Otherwise the fits are made in the same way as in Table 5. Some cases are not constrained (N/C). [c] The generalized correlation being reanalyzed with a free n.

Table 7: Fits to the Evolution of the Photon Fluence for 23 Pulse Decays

	$\Phi(t)$[a]		
Trigger	f_0 (cm^{-2})[b]	τ (s)	χ^2/d.o.f
451	61.4 ± 1.5	4.60 ± 0.19	3.94
647	182 ± 6	4.54 ± 0.20	0.26
829	437 ± 14	2.57 ± 0.12	2.47
1085	128.7 ± 0.5	22.32 ± 0.14	0.349
1141:1	-59 ± 3	2.15 ± 0.10	0.14
1141:2	-81.8 ± 1.8	0.93 ± 0.03	0.99
1625	78.7 ± 0.7	2.17 ± 0.03	0.88
1663	18.6 ± 0.4	0.442 ± 0.023	0.91
2083:1	1850 ± 20	0.659 ± 0.013	2.92
2083:2	99.5 ± 1.3	13.8 ± 0.3	1.47
2156	88.4 ± 1.2	7.41 ± 0.17	1.66
2919	49.5 ± 0.3	8.7 ± 0.7	0.12
3042	156.0 ± 2.2	1.18 ± 0.03	0.84
3345	-592 ± 7	1.193 ± 0.023	0.21
3492	99.9 ± 2.2	0.96 ± 0.04	9.87
3648	138 ± 3	2.46 ± 0.09	1.07
3765	83.5 ± 0.4	3.52 ± 0.03	0.49
3870	95.8 ± 0.6	1.696 ± 0.018	0.37
3954	51.6 ± 0.3	4.48 ± 0.05	0.38
5567	49.4 ± 1.1	1.82 ± 0.08	8.85
6100	95.5 ± 0.5	4.55 ± 0.04	1.09
6630	365 ± 10	1.61 ± 0.07	1.22
7527	243 ± 7	2.63 ± 0.11	1.87

[a]Parameter for the fits to equation (11) with $f_0 = N_0\tau/(n-1)$ and using the n obtained by fitting the light curve, $N(t)$ (see Table 2) in all cases but 1663 for which equation (2) was used with $f_0 = N_0\tau$.

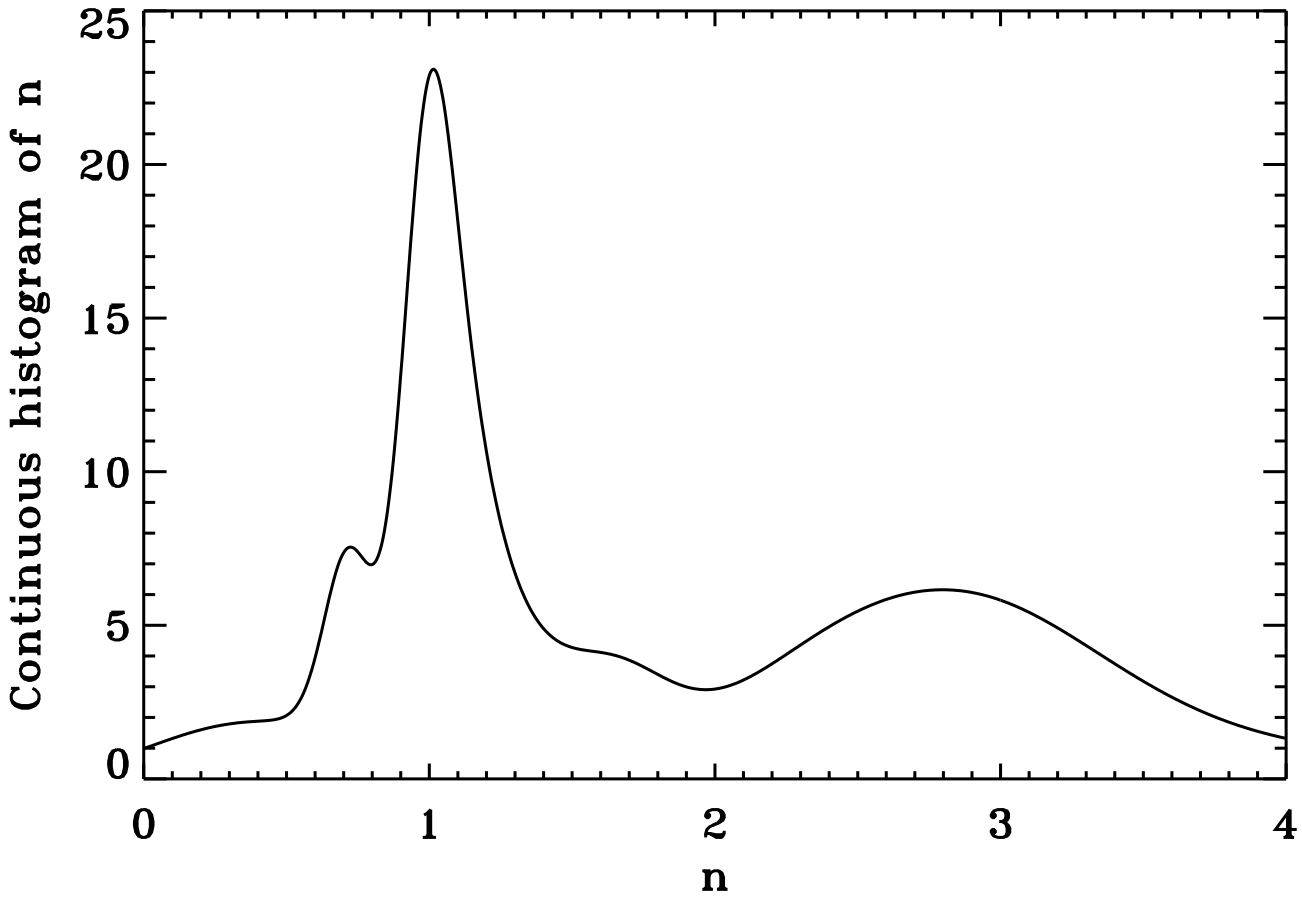

Fig. 1.— Continuous histogram of the power-law exponent, n, in Eq. (10). The histogram is constructed by summing Gaussian functions which have the values of the mean and the variance found from the fits. Note the bimodality in the distribution with peaks at $n \sim 1$ and ~ 3.

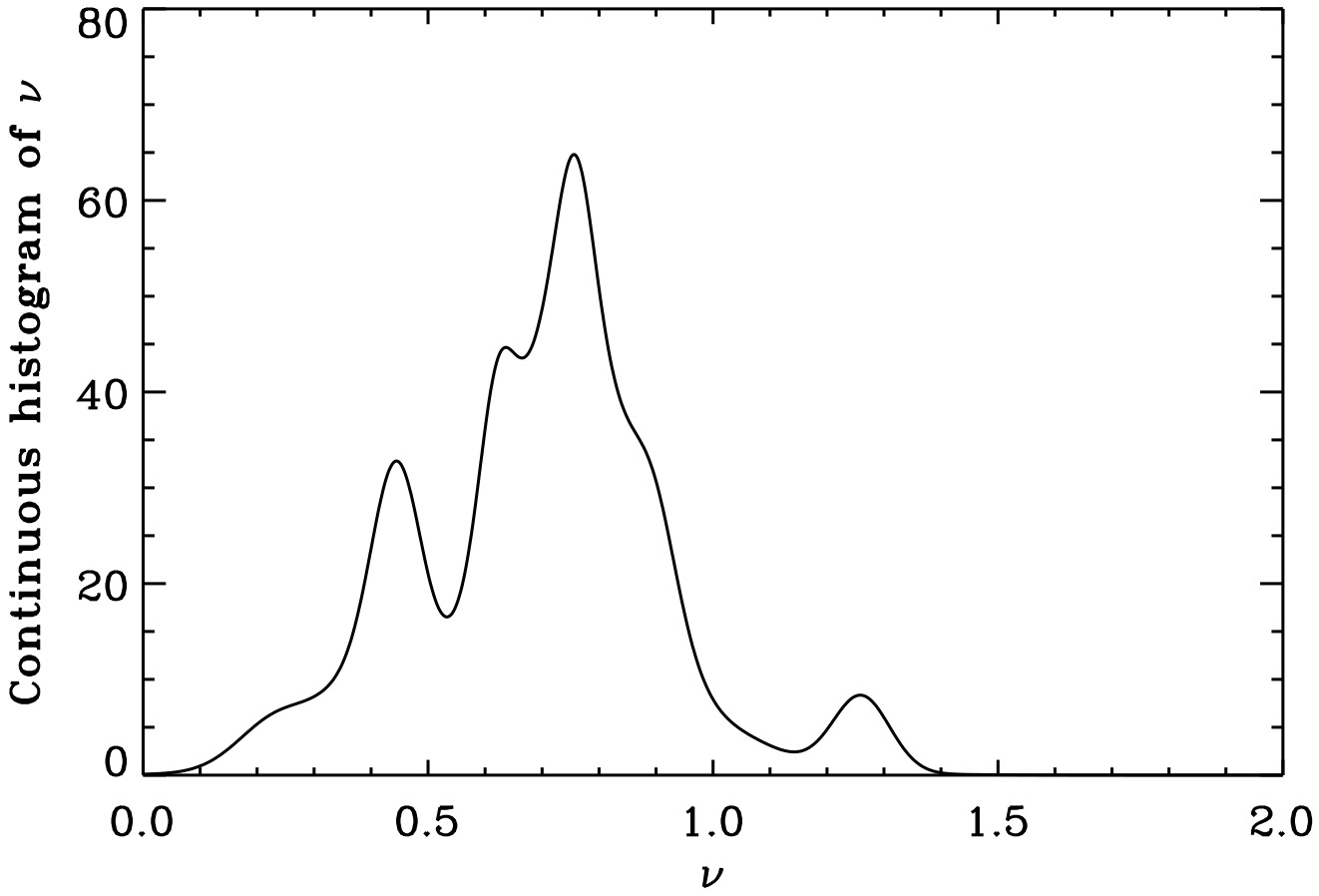

Fig. 2.— Continuous histogram of the peakedness parameter ν, in Eq. (1). See Fig. 1 for details.

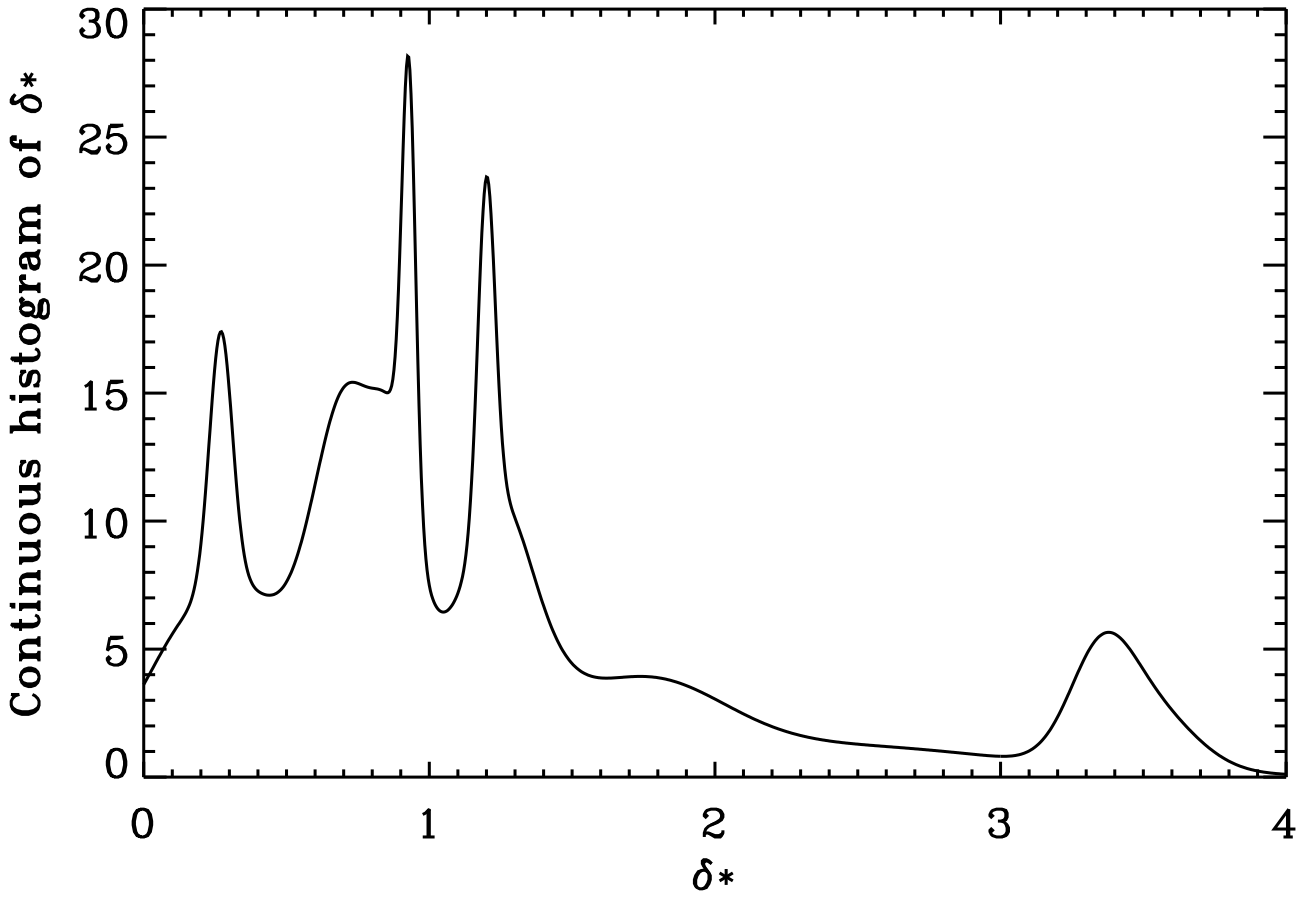

Fig. 3.— Continuous histogram of the exponent, δ_* see Tab. 2.

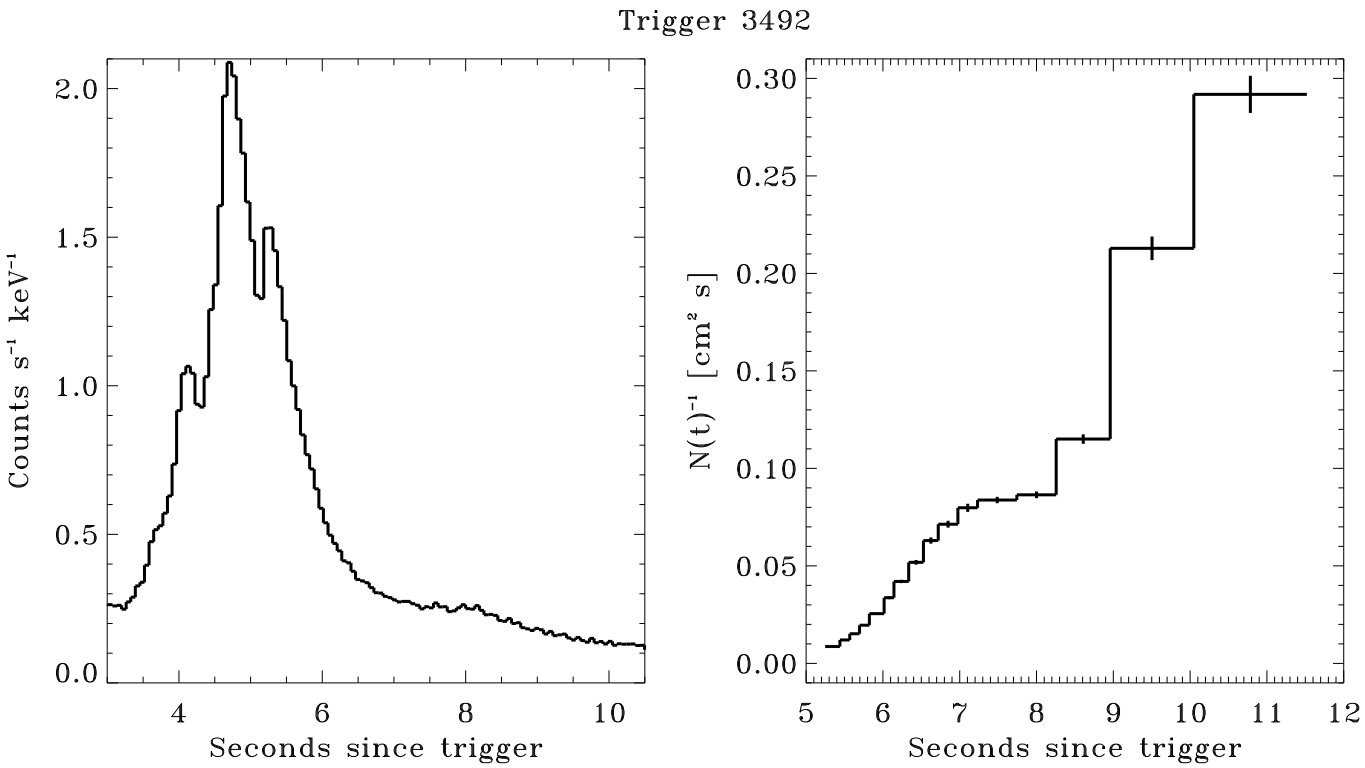

Fig. 4.— The reciprocal photon flux light curve, $N(t)^{-1}$, of GRB950403 (trigger 3492). Only the first 10 bins out of the total 16 are used in the study, motivated by the additional feature beyond in 10.

Fig. 5.— The spectral and temporal behaviors of the GRB pulses in the sample. The left-hand panel in every horizontal strip shows the DISCSC data (all four energy channels are used) and indicates the time interval studied (also see Table 1). The second panel, from the left, shows the light curve with the LAD HERB data in the chosen time binning. The best fit is indicated with a solid curve (see Table 2 for parameters). The two right-hand panels show the correlations, the HIC $E_{\rm pk}(N)$ in panel 3 and the HFC $E_{\rm pk}(\Phi)$ in panel 4. Case (i) (i.e., $n = 1$) is represented by the solid line in panel 3 (the power law HIC $E_{\rm pk}(N)$) and the dashed line in panel 4 (the exponential HFC $E_{\rm pk}(\Phi)$). Case (ii) is represented by the dashed curves in the two panels, the generalized HIC $E_{\rm pk}(N)$ in panel 3 and the exponential HFC $E_{\rm pk}(\Phi)$ in panel 4. Finally, case (iii) is represented by the solid curves in the two panels, the power law HIC $E_{\rm pk}(N)$ in panel 3 and the generalized HFC $E_{\rm pk}(\Phi)$ in panel 4. See the text for details. The overlying data point in the HIC diagram for trigger 1441:2 is marked by a larger symbol.

Fig. 6.— The temporal behaviors of the GRB pulses in the sample regarding (i) the photon fluence, Φ, with the best fit marked by a solid curve (see Table 7 for parameters) and (ii) the peak energy, $E_{\rm pk}$, with the best fit marked by a dashed curve (see Table 2 for parameters)

Trigger 451

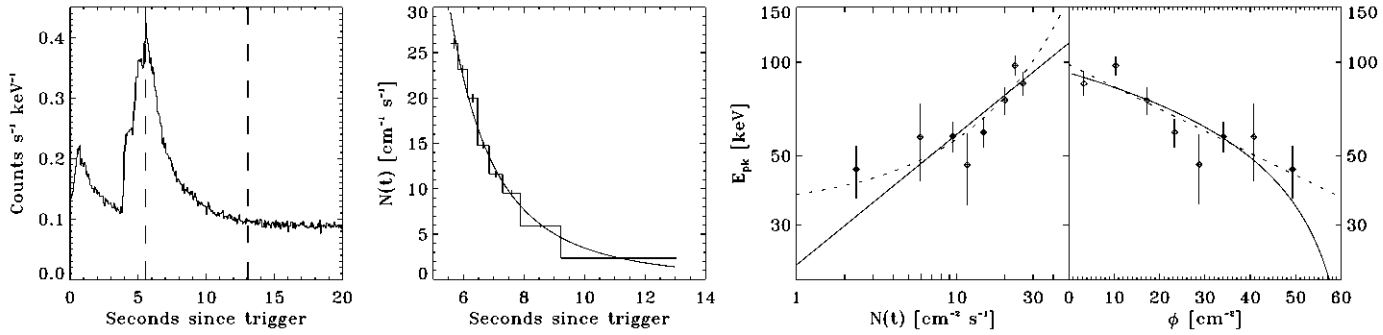

Trigger 647

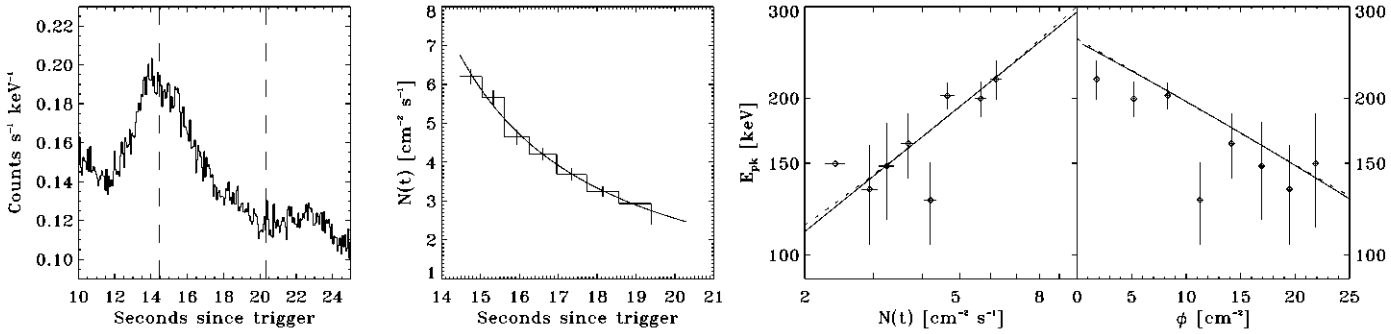

Trigger 829

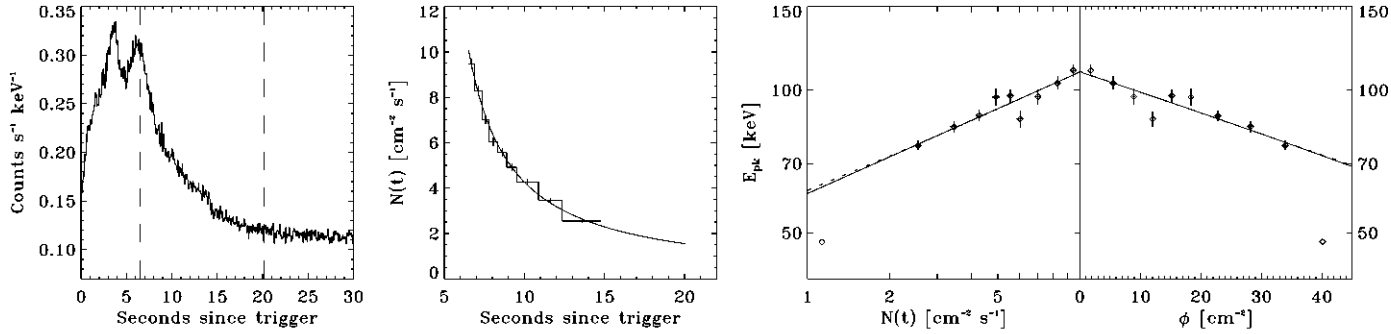

Trigger 1085

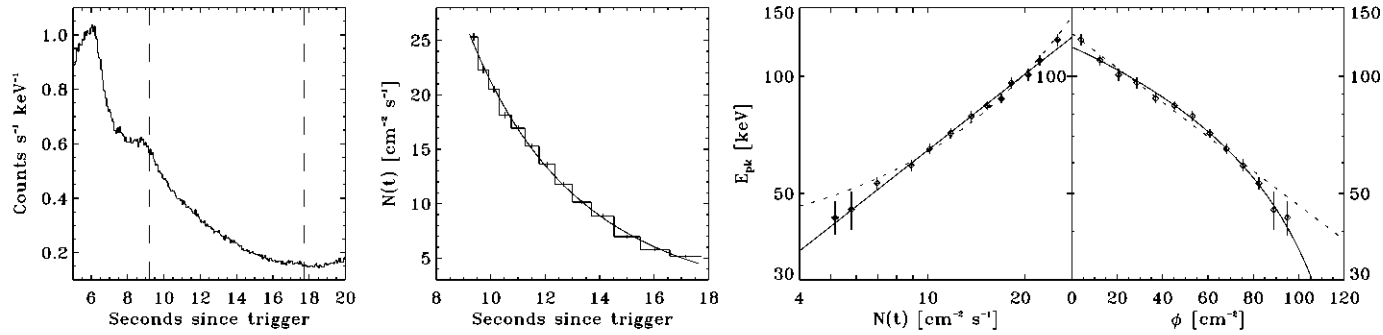

Trigger 1141:1

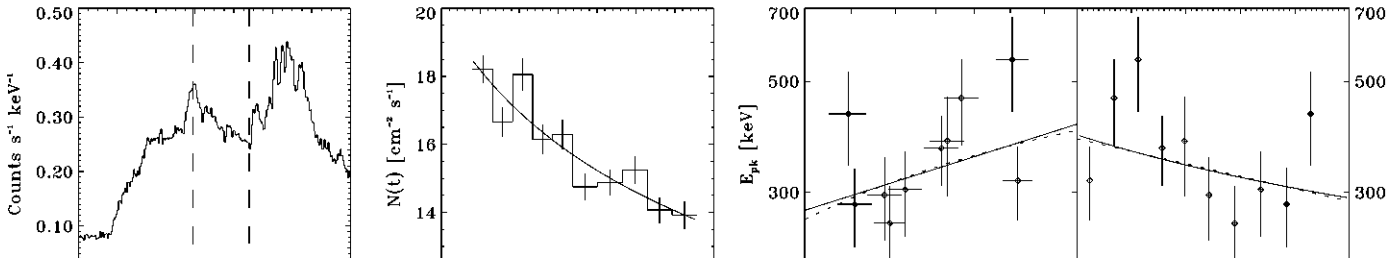

Trigger 1141:2

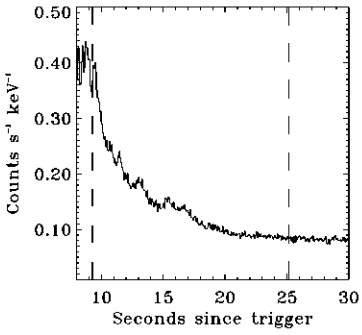

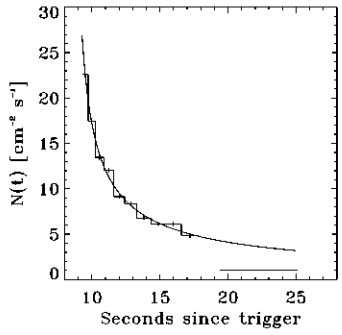

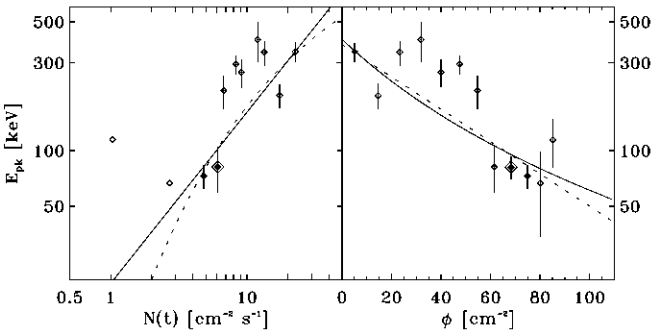

Trigger 1625 *

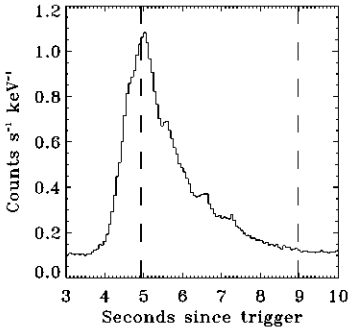

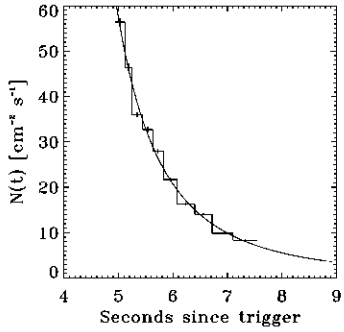

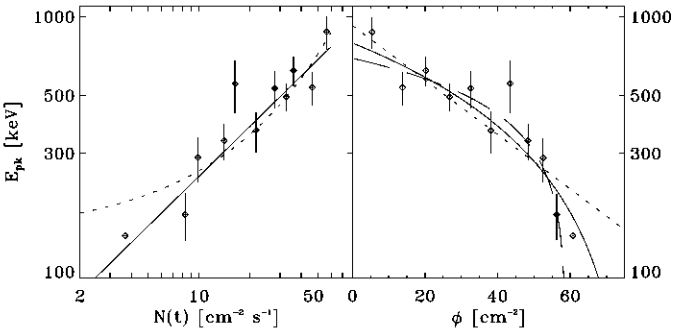

Trigger 1663

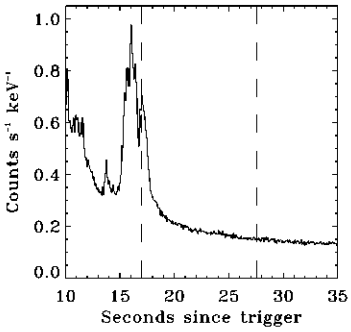

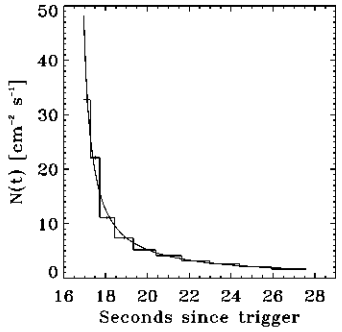

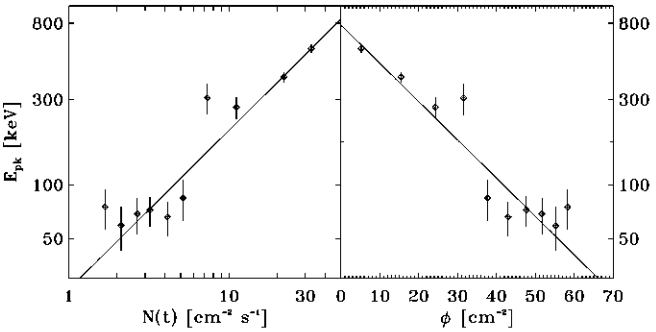

Trigger 2083:1

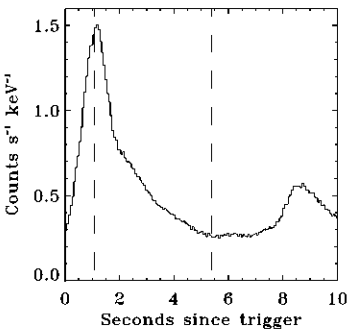

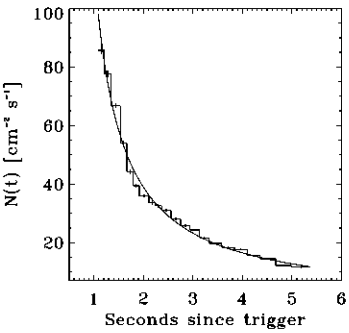

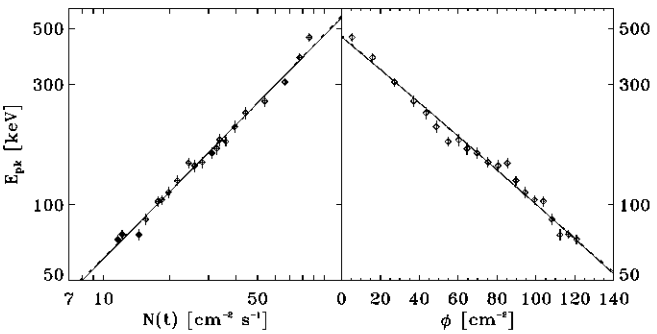

Trigger 2083:2

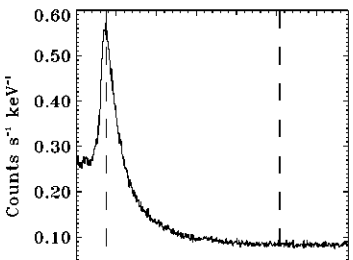

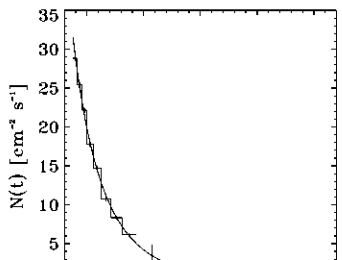

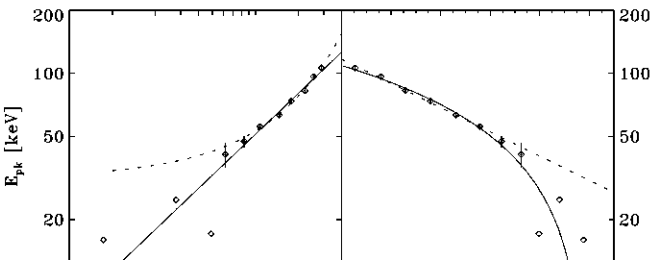

Trigger 2156

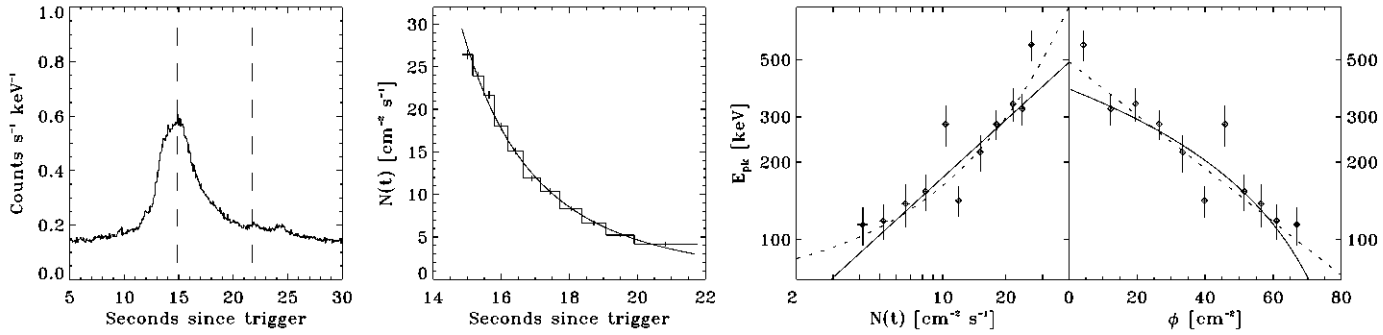

Trigger 2919

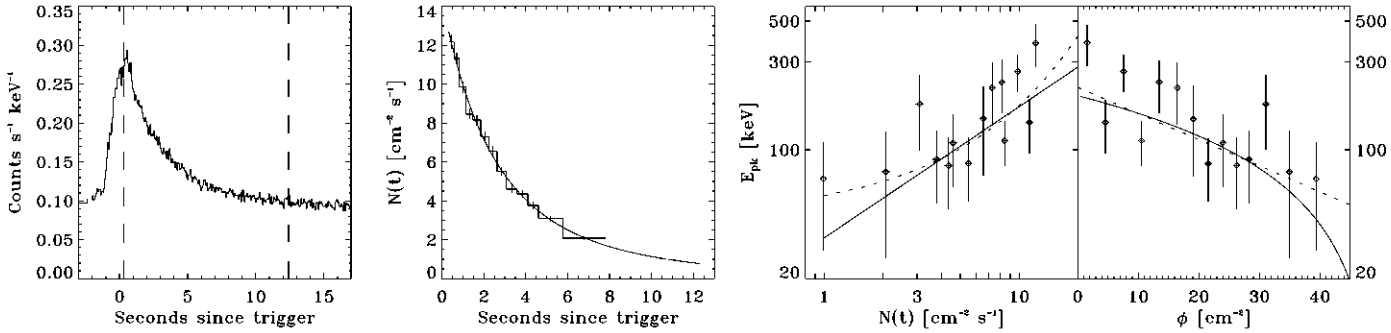

Trigger 3042

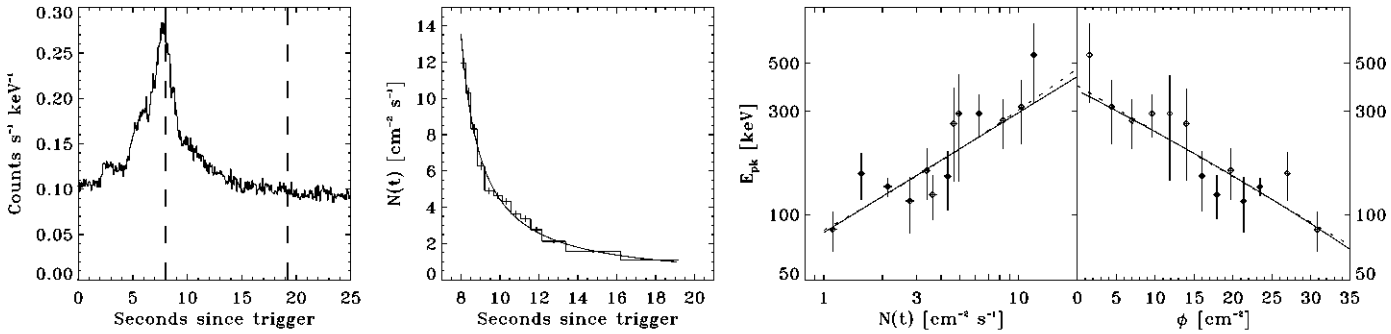

Trigger 3345

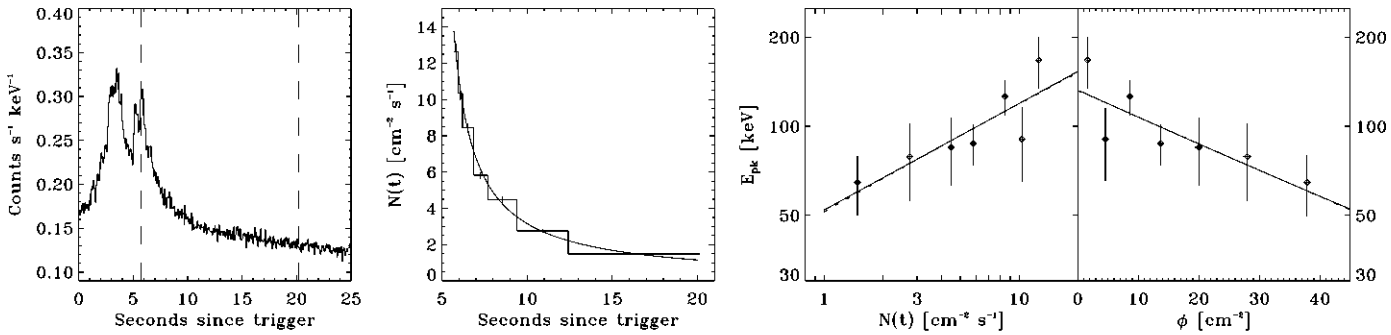

Trigger 3492 *

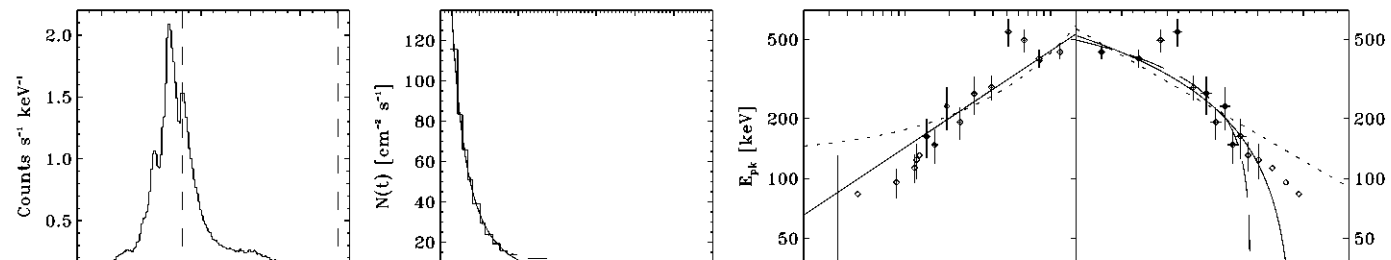

Trigger 3648

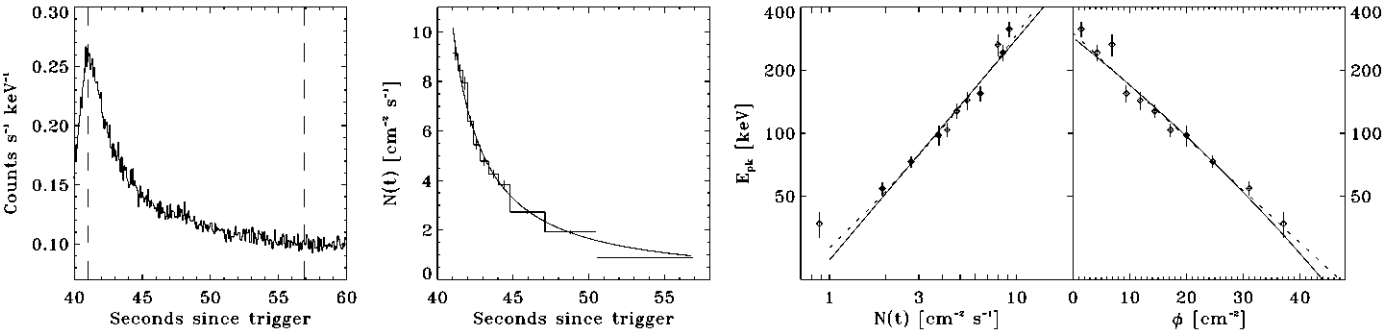

Trigger 3765 *

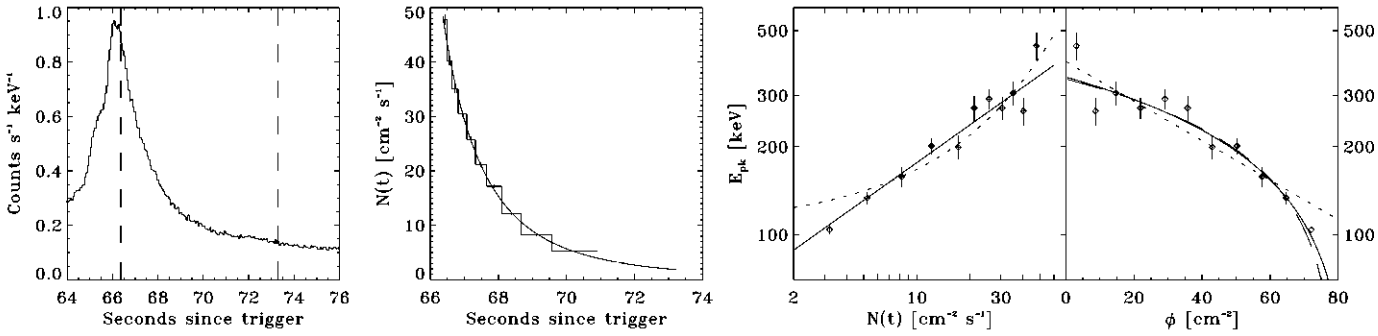

Trigger 3870

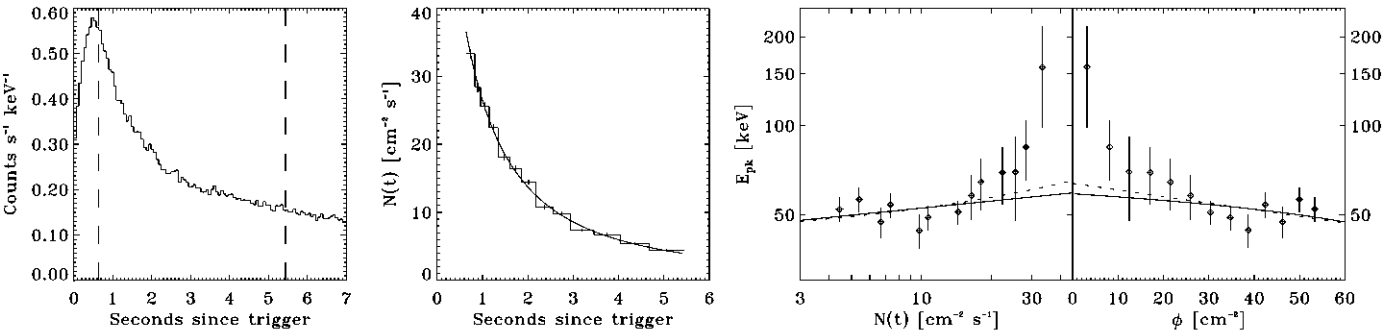

Trigger 3954

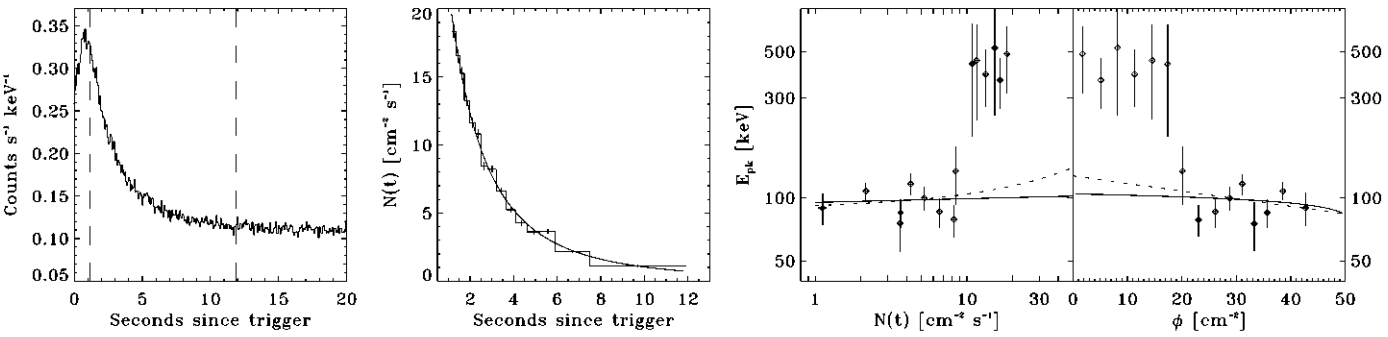

Trigger 5567 *

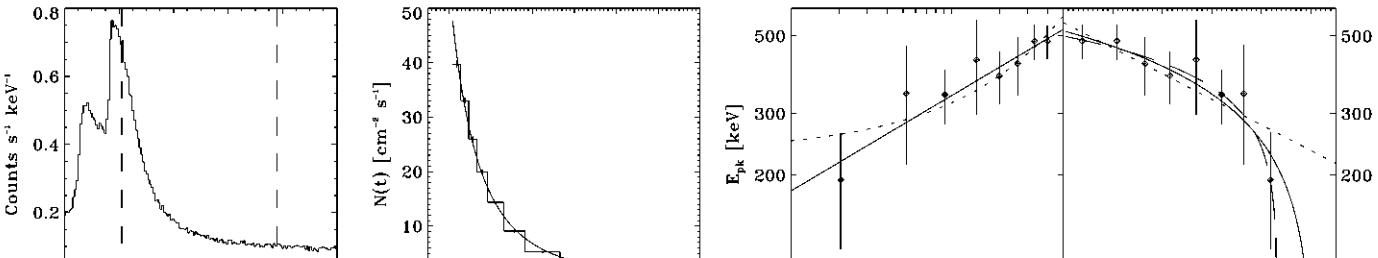

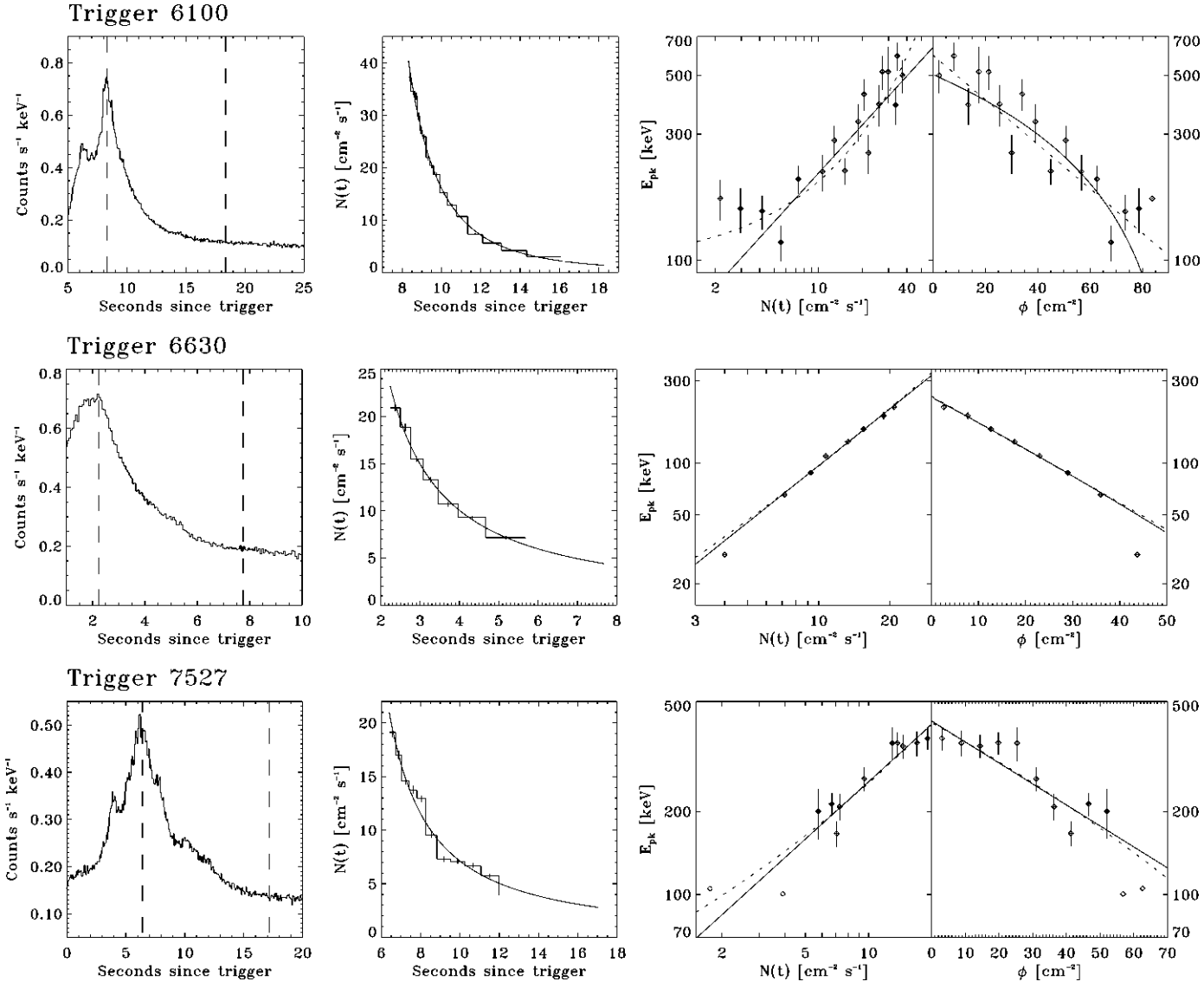
Trigger 6100
Counts s⁻¹ keV⁻¹
Seconds since trigger
N(t) [cm⁻² s⁻¹]
Seconds since trigger
E_pk [keV]
N(t) [cm⁻² s⁻¹]
φ [cm⁻²]
Trigger 6630
Counts s⁻¹ keV⁻¹
Seconds since trigger
N(t) [cm⁻² s⁻¹]
Seconds since trigger
E_pk [keV]
N(t) [cm⁻² s⁻¹]
φ [cm⁻²]
Trigger 7527
Counts s⁻¹ keV⁻¹
Seconds since trigger
N(t) [cm⁻² s⁻¹]
Seconds since trigger
E_pk [keV]
N(t) [cm⁻² s⁻¹]
φ [cm⁻²]

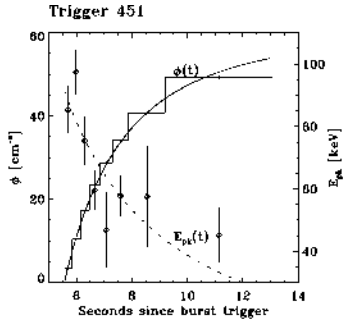
Trigger 451
ϕ(t)
E_pk(t)
ϕ [cm⁻²]
E_pk [keV]
Seconds since burst trigger

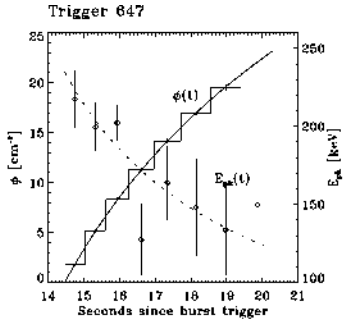
Trigger 647
ϕ(t)
E_pk(t)
ϕ [cm⁻²]
E_pk [keV]
Seconds since burst trigger

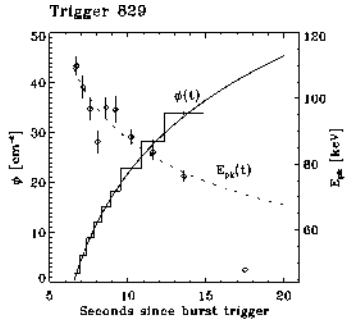
Trigger 829
ϕ(t)
E_pk(t)
ϕ [cm⁻²]
E_pk [keV]
Seconds since burst trigger

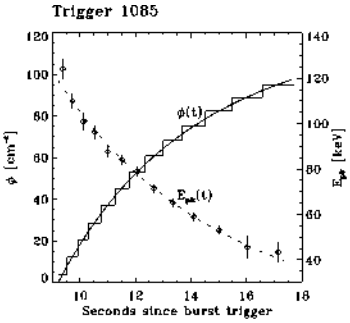
Trigger 1085
ϕ(t)
E_pk(t)
ϕ [cm⁻²]
E_pk [keV]
Seconds since burst trigger

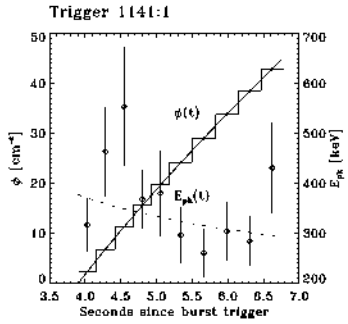
Trigger 1141:1
ϕ(t)
E_pk(t)
ϕ [cm⁻²]
E_pk [keV]
Seconds since burst trigger

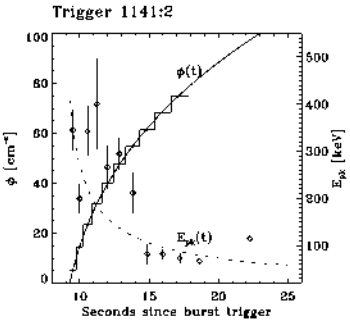
Trigger 1141:2
ϕ(t)
E_pk(t)
ϕ [cm⁻²]
E_pk [keV]
Seconds since burst trigger

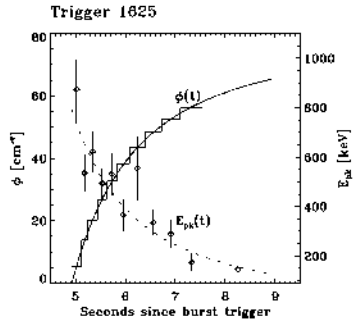
Trigger 1625
ϕ(t)
E_pk(t)
ϕ [cm⁻²]
E_pk [keV]
Seconds since burst trigger

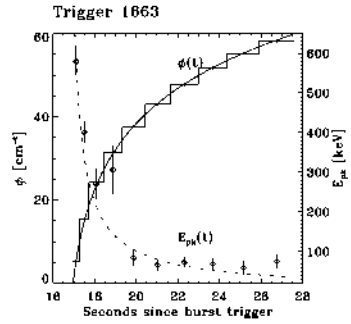
Trigger 1663
ϕ(t)
E_pk(t)
ϕ [cm⁻²]
E_pk [keV]
Seconds since burst trigger

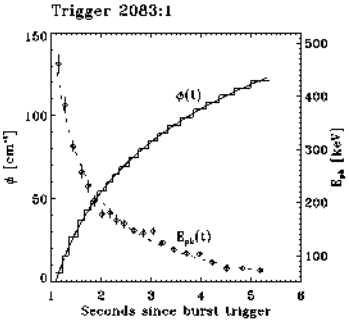
Trigger 2083:1
ϕ(t)
E_pk(t)
ϕ [cm⁻²]
E_pk [keV]
Seconds since burst trigger

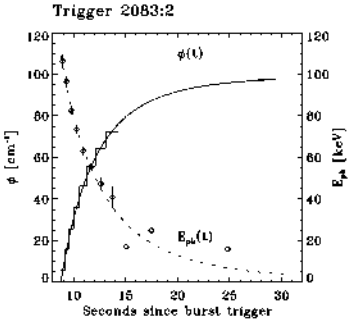
Trigger 2083:2
ϕ(t)
E_pk(t)
ϕ [cm⁻²]
E_pk [keV]
Seconds since burst trigger

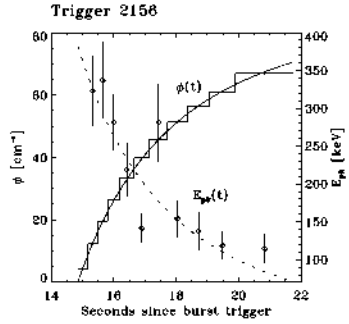
Trigger 2156
ϕ(t)
E_pk(t)
ϕ [cm⁻²]
E_pk [keV]
Seconds since burst trigger

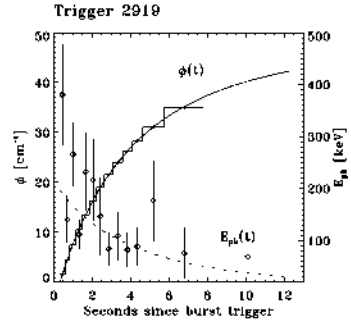
Trigger 2919
ϕ(t)
E_pk(t)
ϕ [cm⁻²]
E_pk [keV]
Seconds since burst trigger

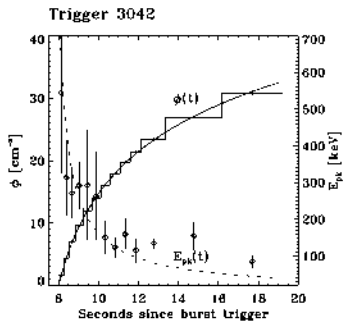
Trigger 3042
ϕ(t)
E_pk(t)
ϕ [cm⁻²]
E_pk [keV]
Seconds since burst trigger

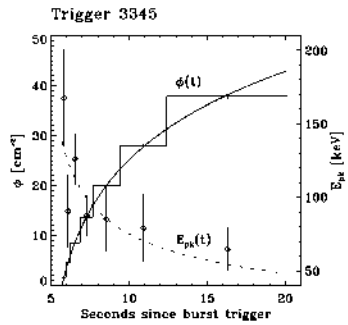
Trigger 3345
ϕ(t)
E_pk(t)
ϕ [cm⁻²]
E_pk [keV]
Seconds since burst trigger

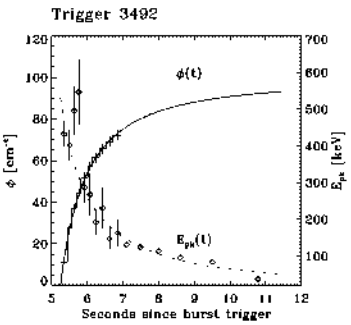
Trigger 3492
ϕ(t)
E_pk(t)
ϕ [cm⁻²]
E_pk [keV]
Seconds since burst trigger

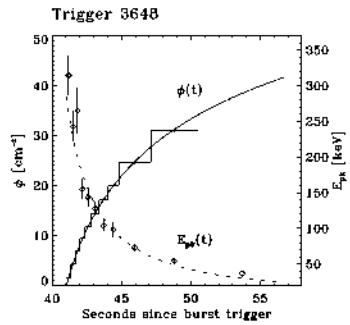
Trigger 3648
ϕ(t)
E_pk(t)
ϕ [cm⁻²]
E_pk [keV]
Seconds since burst trigger

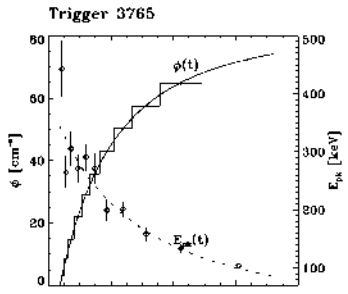
Trigger 3765
ϕ(t)
E_pk(t)
ϕ [cm⁻²]
E_pk [keV]

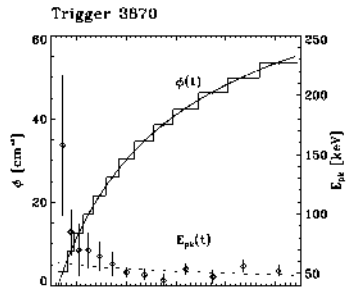
Trigger 3870
ϕ(t)
E_pk(t)
ϕ [cm⁻²]
E_pk [keV]

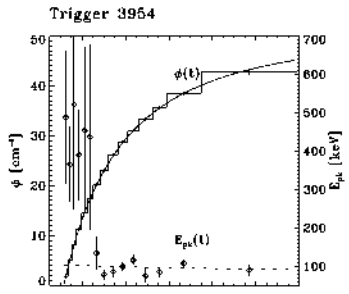
Trigger 3954
ϕ(t)
E_pk(t)
ϕ [cm⁻²]
E_pk [keV]

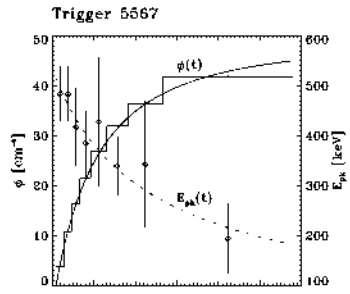
Trigger 5567
ϕ(t)
E_pk(t)
ϕ [cm⁻²]
E_pk [keV]

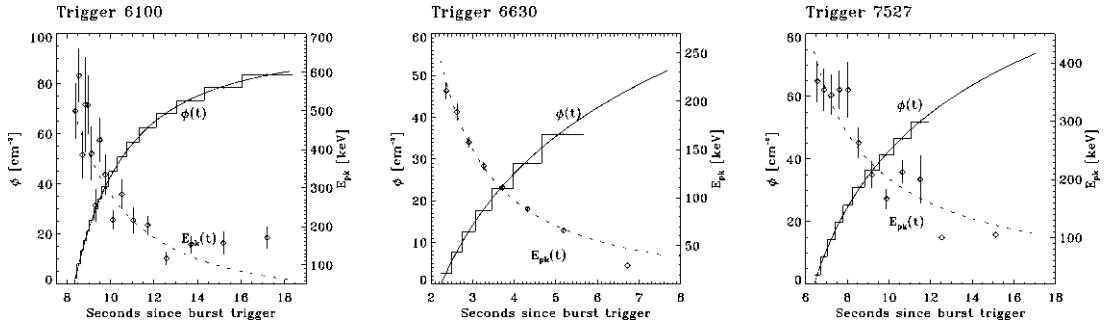
Trigger 6100
Trigger 6630
Trigger 7527
ϕ(t)
E_pk(t)
ϕ [cm⁻²]
E_pk [keV]
Seconds since burst trigger